ELEVENTH EUROPEAN ROTORCRAFT FORUM

Paper No. 27

THE AERODYNAMIC CALCULATION OF
COUNTER ROTATING COAXIAL ROTORS

Herbert Zimmer

Dornier GmbH
Friedrichshafen, FRG

September 10-13, 1985
London, England

THE CITY UNIVERSITY, LONDON, EC1V 0HB, ENGLAND

THE AERODYNAMIC CALCULATION OF COUNTER ROTATING COAXIAL ROTORS

H. Zimmer

Dornier GmbH, Aerodynamics Department
Project Aerodynamics Group
Friedrichshafen, FRG

Abstract

For the calculation of the loading, vibrations and the insta-
bility of counter rotating coaxial helicopter rotors and pro-
pellers, the knowledge of the aerodynamic forces on each blade
element at every time step is essential. For the aerodynamic
calculation of these interfering rotors a method was developed,
which on hand should be inexpensive in computer time and on the
other hand should represent the complicated flowfield as rea-
listically as possible. The method should apply in hovering and
forward flight with uniform and nonuniform inflow. Also the
method is built up in such a way that besides the relatively
lightly loaded helicopter rotors also heavily loaded single
rotating and counter rotating propellers can be calculated.
Because of the inherent aerodynamic advantages the coaxial
arrangement is becoming more and more important in this field.

Notation

a	Distance, non-dimensional pitch oscillation amplitude $= \delta_{max}/(H/c)$
A_1	Disk area of rotor 1, $A_1 = A_2$
AF	Activity Factor $= 100.000/16 \int_{0.2}^{1.0} c/2R(r/R)^3 \, d(r/R)$
AR, Λ	Aspect Ratio
b	Span
c	Chord length
c_{75}	Chord length at 0,75 Radius
c_D	Drag coefficient
c_{d_i}	Coefficient of induced drag
c_l	Lift coefficient
c_L	Rotor rolling moment coefficient $= L/(\rho \pi \Omega^2 R^5)$
c_M	Rotor pitching moment coefficient $= M/(\rho \pi \Omega^2 R^5)$
c_p	Rotor power coefficient $= P/(\rho n_s^3 D^5)$
c_p'	Oscillating wing power coefficient $= P/(\rho/2 \, V_b^3 H b)$
CPU	Central Processing Unit
C_Q	Rotor torque coefficient $= M_Q/(\rho \pi \Omega^2 R^5)$
CRP	Counter Rotating Propeller
C_T	Rotor thrust coefficient $= T/(\rho n_s^3 D^4)$
c_T'	Rotor thrust coefficient $= T/(\rho \pi \Omega^2 R^4)$
D	Rotor diameter, Drag
D_{RF}	Drag of oscillating wing
E	Wing element
$F.M.$	Figure of Merit $= \sqrt{2/\pi} \, c_T^{1,5}/c_p = 0,707 \, c_T'^{1,5}/c_Q$

H	Height, oscillation amplitude of wing
i	Number of time step
IA	Influence Area on second rotor
J	Advance ratio $= V/n_S D$
L	Rotor rolling moment, wing lift
L_{RF}	Lift of oscillating wing
$\dot{m}$	Mass flow through rotor plane
M	Rotor pitching moment
M_Q	Rotor torque
n	Revolutions per minute, number of wing elements
n_S	Revolutions per second
P	Power, station point
r	Radial station
R	Rotor radius
r_c	Vortex core radius
R_w/R	Contraction of tip vortex
SRP	Single Rotation Propeller
T	Rotor thrust
$V, V_o(V_x, V_y, V_z)$	Onset flow (Components)
$V_{d1,2}$	Velocity through Rotor 1,2
ΔV_{d2}	Downwash correction in plane of second rotor
ΔV_{d2B}	Downwash correction at blade of second rotor
$V_{m1,2}$	Mean downwash velocity of Rotor 1,2
V_{mx}	Average value of mean downwash velocities of both rotors
V_{mxo}	Average downwash velocity according to axial momentum
V_R	Resulting velocity
V_{RF}	Onset flow of oscillating wing
V_t	Swirl velocity
$w_i(\Delta w_i)$	Induced velocity (increment)
w_ξ	Oscillation velocity
x,y,z	Cartesian coordinate system of rotor
x_B, y_B, z	Coordinate system of blade
z_b	Number of blades
Z_w/R	Axial displacement of tip vortex
α	Angle of attack
α_{eff}	Effective angle of attack
α_i	Induced angle of attack
γ	Non-dimensional circulation $= c_L \cdot c/2b$
$\Gamma, \Gamma_G, \Gamma_F$	Circulation, bound, free
δ	Pitch oscillation angle, inflow angle of blade element
ε	Inflow angle of oscillating wing
ε_s	Swirl angle
η	Non-dimensional span
η, y, ξ	Cartesian coordinate system of oscillating wing
η_V	Propulsive efficiency $= T \cdot V/P = J \cdot c_T/c_P$
ϑ	Twist angle
ϑ_{75}	Blade chord angle at 0,75 Radius
ρ	Density of medium
σ	Solidity $= z_b \cdot c_{75}/\pi R$
ψ	Phase angle
ω, Ω	Frequency
$\bar{\omega}$	Reduced frequency $= \omega \cdot c/V$

1.   INTRODUCTION

In order to calculate the loading, vibrations and the insta-
bility of counter rotating coaxial helicopter rotors and pro-
pellers, the aerodynamic forces on each blade element must be
known in every time step. The whole task of the dynamic cal-
culation of a coaxial rotor or propeller is not yet completed,
therefore here only the aerodynamic part of the calculation of
the rotor forces will be discussed.

Because of the strong mutual rotor interference the calculation
of the forces of coaxial rotors is a quite complex aerodynamic
problem. To solve this problem a method was to be developed,
which on one hand would use as little computer time as possible
in order to afford many time steps in the dynamic rotor cal-
culation, but on the other hand would represent the complicated
physical flow field as realistically as possible to catch the
main effects.

First of all a review was made of the available literature on
the calculation of coaxial rotors (/1/ - /7/). In the theories
which use the local momentum concept (/1/ - /6/), each rotor-
blade is essentially treated as a series of elementary wings,
each of which has an elliptical circulation distribution. The
forces of interest are calculated from the instantaneous momen-
tum balance of fluid and blade elementary lift at any local
station point in the rotor plane. To represent the timewise
variation of the local induced velocities following a blade
passage a more or less sophisticated vortex theory has to be
introduced. A vortex strip theory for coaxial rotors in hover
has also been reported in /7/.

After consideration of these theories a method was built up
according to the curved lifting line - vortex wake - blade ele-
ment - momentum - concept in such a way, that besides the rela-
tively lightly loaded helicopter rotors also heavily loaded
single rotating and counter rotating propellers can be calcula-
ted (Fig. 1). Also nonuniform inflow was to be treated. The
method was tested first on fixed and oscillating wings, then on
single rotating and counter rotating rotors and propellers. Re-
sults will be shown for two fixed and one oscillating wing,for
a single and counter rotating helicopter rotor in hover and for
single and counter rotating advanced General Aviation propel-
lers at very high advance ratio.

2.   OUTLINE OF THE ADOPTED METHOD

Because of the complexity of the problem different aspects of
the calculation procedure were tested first on fixed and oscil-
lating wings, since a blade of a hovering rotor is comparable
in some respects with a fixed wing in general onset flow and a
blade of an advancing rotor in skewed flow resembles to some
degree an oscillating wing.

2.1   Local aerodynamic characteristics

To represent the local aerodynamic characteristics of the blades as accurately as possible, the lift and drag of several definition airfoils can be introduced as 2- or 3-dimensional arrays depending on angle of attack, Mach number, Reynolds number, or momentum coefficient (for blown airfoils), or cavitation number (for water propellers).

2.2   Curved lifting line

Since swept blade tips or swept propeller blades were also to be taken into account and since the systematic error in representing the rotorblade by a set of elementary elliptical wings according to Fig. 2 (see /1/) was to be avoided, the blade element - curved lifting line - vortex wake - concept according to Fig. 3 was introduced for a wing in general onset flow. In the calculation of the downwash distribution according to Fig. 3 a second term was introduced in the brackets, which accounts for the effect of the swept lifting line. The set of equations according to general wing theory is solved iteratively until a stable distribution of the induced downwash (Fig. 3) is obtained. After 8 - 12 iterations the variation in the results is less than 1 %.

2.3   Blade-vortex encounter

In vortex theories a problem arises, when the distances between trailing vortices and local station points on the blades are very small. In this case usually numerical instabilities occur. This problem is especially severe in the case of a coaxial counter rotating rotor, because it happens periodically, that the blades of the second rotor encounter and cut the vortex wakes of the blades of the first rotor. To avoid numerical problems, all trailing vortices are represented according to the LAMB-Vortex concept /8/ (Fig. 4). A suitable core radius is the smallest distance between a local station point on the blade and the adjacent trailing vortex.

2.4   Calculation of fixed wings

First the method mentioned above was tested on a fixed rectangular wing as in /1/ (Fig. 2). The results for different numbers of station points are compared with the MULTHOPP-theory in Fig. 5. The results show no systematic deviation and the differences for different discretizations in lift distribution and force coefficients are quite small.

In Fig. 6 the results obtained for a swept tip wing are compared with the results according to vortex lattice theory. The distributions of local induced drag and lift coefficient together with the local circulation differ very little and the force coefficients for different discretizations are all within 2,3 % of the vortex lattice values.

2.5 · Calculation of an oscillating wing

Then, as a pre-check for the rotor performance calculation, and expecially to identify the difference in performance with an instationary and a quasi-stationary vortex wake, the performance calculation of an oscillating swept tip wing was carried out for the case in which the oscillating wing extracts power out of the fluid. Fig. 7 shows the representation of an oscillating wing. In Fig. 7 a) the instationary wake for the time step i = 3 is depicted with up to 3 instationary shed vortices, which contain the differences in bound circulation between the current and the previous time step respectively. Fig. 7 b) and c) denote how the time steps are counted and how the oscillation velocity is introduced into the blade element concept.

When a new time step is begun, the calculation starts with the results obtained in the previous time step. So the following time steps need only about 60 % of the computer time required for the first step.

In Fig. 8 the power coefficient of an oscillating wing at high pitch oscillation ($\pm$ 17°) - i. e. the ratio of the extracted power by the wing to the energy content of the swept streamtube - is compared with results gained by two dimensional flutter theory (reduced by the lift slope ratio of this specific wing compared with the two dimensional value) in dependence of reduced frequency. These results show on one hand a quite reasonable correlation with flutter theory, on the other hand they indicate, that the difference in the results for an instationary or a quasi-stationary wake is only 2 - 3 %. It is therefore concluded, that the coaxial rotor calculations can be made with quasi-stationary wakes and with practically no significant loss in accuracy at only a fraction in computer time.

Also calculations were made for cases in which the wing imparts energy to the fluid (oscillating wing propulsion). In these cases also reasonable results were obtained.

2.6 Coaxial Rotor Calculation

Using the described basic procedures the coaxial rotor calculation method was built up according to the curved lifting line - vortex wake - blade element - momentum - concept. The rotorblades are represented by a number of blade elements (Fig. 9) which work under twodimensional flow conditions. The threedimensionality of the rotor flow field is represented by the induction of the whole wake vortex field which varies with every time step. Similar to /9/ every blade has a relatively short vortex wake consisting of several elementary vortices emanating at the blade element boundaries. A rolled-up tip vortex extends further downstream up to a certain length specified by dissipation considerations. Only the radial contraction of the

tip vortices is given for the first and second rotor using information from /5/, /7/, /9/ together with the change in axial displacement due to the following blade. The radial contraction of the elementary wake vortices being proportional to the respective tip vortex a basic wake vortex model is built up in every time step for a given onset flow. So Fig. 10 shows the basic vortex model of an advancing two blade coaxial helicopter rotor in three time steps. The fourth time step would be identical to the first one.

The calculation procedure in every time step is outlined in Fig. 11. At a certain station point P (Fig. 11 a) a wake vortex element AB induces a certain velocity increment according to the BIOT-SAVART law. The totality of all wake vortices produces a certain induced velocity at the point P and together with the onset flow and the geometric properties the effective angle of attack of the blade element denoted by P is specified. With the effective flow direction and aerodynamic characteristics given at every blade element, the aerodynamic forces can be calculated according to Fig. 11 b) for all blade elements. With the effective flow direction at every blade element now being known a correction of the basic vortex model according to Fig. 10 is introduced in such a way that the axial displacement of all blade wake vortices is adjusted according to the downwash distribution of the generating blade.

The rotor forces and moments at the considered time step are found by integrating all blade element forces according to Fig. 11 c). An overview of the calculation procedure is given in Fig. 11 d). Essentially, in an iterative procedure at every time step the induced downwash distribution at each blade on each rotor is determined as illustrated in Fig. 12 a). This is the base for the force calculation.

Since the blade wakes are represented quite realistically, the tip effects and the blade - vortex - encounters show a realistic behaviour, but the swirl and downwash distributions have to be corrected for truncation errors because only short vortex wakes are considered.

The swirl velocity V_t is corrected according to Fig. 11 b) with the Eulerian turbine equation, for the distribution of the swirl velocity must correspond to the rotor torque distribution.

The downwash distributions are corrected in two ways. First the downwash distribution of the second rotor is corrected according to Fig. 12 b) within the influence area IA, where the downwash of the first rotor hits the rotorplane of the second rotor. The downwash correction is such, that the downwash distribution of the first rotor is increased according to the downwash contraction (ΔVd_{2i}) and that for the momentary blade position on the second rotor the actual downwash correction is interpolated (ΔVd_{2iB}). Secondly, the downwash distributions must

be corrected in such a way, that the rotor thrust is compatible with axial momentum theory. As is shown in Fig. 12 c) the average of the mean downwash velocities of both rotors has to fulfill the axial momentum equation.

After all necessary results have been found in every time step, the overall rotor coefficients are determined according to Fig. 12 d).

3.   CALCULATED EXAMPLES

With the described method several single and counter rotating rotors were calculated and compared with experimental and other theoretical results. First, results of a full-scale helicopter rotor in hover are shown, and later results of propellers at high advance ratios will be presented.

3.1   Helicopter rotor

First the full scale helicopter rotor according to /10/ was considered. The rotor geometry is depicted in Fig. 13. The blades of the two blade rotors have relatively thick symmetrical airfoils and are untwisted. The aerodynamic characteristics of the most inboard and the most outboard definition airfoil are shown in Fig. 14. It has been extracted out of wind tunnel results.

3.1.1 Single rotating rotor

This rotor was first calculated as a single rotation rotor. The definition of the tip vortex can be seen in Fig. 15. Fig. 16 compares the calculated and measured performance. The theoretical values lie within around 2 % of the measurement except in the case of maximum thrust, even with the relatively crude representation of the rotor. The hover efficiency according to Fig. 17 is similar in trend. For the point S of maximum efficiency in Fig. 18 the distributions for the local lift coefficient and downwash are shown, and in Fig. 19 the wake vortex system together with the coefficients of interest. This case took 2 sec CPU-time on a IBM-3083 computer. In this stationary case only one time step is needed.

3.1.2 Counter rotating rotor

In the calculation the blade angles were always varied such that each rotor would absorb the same power (i. e. trimmed condition). Fig. 20 shows the definition used for the tip vortices. The comparison of the calculated and measured performance according to Fig. 21 shows good agreement only for low and medium thrust (curve with point B). For high thrust the calculation falls below the measured values. In order to represent the measurements better in the high thrust cases a modification of the downwash correction according to Fig. 12 c) was studied

(curve with point A). As indicated in the hover efficiency re-
sults of Fig. 22, a good correlation with measurements for high
thrust loading is achieved, when the mass flow of the first ro-
tor is smaller than that through the influence area IA of the
second rotor for the present contraction according to Fig. 20,
i. e. a relatively strong radial inflow between the rotors is
present at high thrust (arrows in Fig. 22). These results seem
to indicate that in hover a variable contraction of the tip
vortex of the first rotor dependent on thrust loading should be
incorporated into the calculation procedure.

In Fig. 23 the distributions of the local lift coefficients and
downwash are shown for the two rotors in condition A which cor-
responds to the theoretical maximum in hover efficiency. Since
the second rotor works in the downwash field of the first
rotor, it produces less thrust than the first rotor for the
same absorbed power. Its thrust share of around 80 % of the
first rotor corresponds with the results in /6/. One reason for
the relatively low hover efficiency of 61 % can also be conclu-
ded from Fig. 23, i. e. the negative lift in the inner part of
the second rotor which is due to the untwisted blades.

Fig. 24 shows the wake model in working condition B (Fig. 22).
The side view (Fig. 24 a) shows that in spite of the lower mean
downwash velocity on the first rotor, its tip vortex moves
faster downstream than that of the second rotor. In Fig. 24 b)
the wake model is depicted in three time steps. In these steps
the thrust variation is between + 1 and - 1,4 % of the mean
value, the torque variation is between - 3,7 and + 2,5, which
causes an appreciable vibratory loading for the drive system.

3.2   **Propeller**

The growing interest in propeller propulsion in recent years is
based on its propulsive advantages as can be seen in Fig. 25
/11/. Here especially the advantage of high speed coaxial pro-
peller propulsion over current turbofan propulsion is evident.
In the following some results of single and counter rotating
General Aviation propellers for M = 0.6 cruise Mach number are
shown (compare points A and C in Fig. 25).

3.2.1   Single rotating propeller

First a high performance single rotation General Aviation pro-
peller is considered /12/, the blade definition of which is
shown in Fig. 26. The blades are built up using the advanced
transonic airfoils P1 - P4 /13/, /12/. The aerodynamic charac-
teristics of one of the definition airfoils (P1) is given in
Fig. 27. For the cruise condition (point A in Fig. 25) with a
very high advance ratio the influence of different discretiza-
tions can be seen in Fig. 28. The relatively crude representa-
tion according to Fig. 28 b) yields differences in the results
well below 0,2 % and uses 60 % of the computer time when compa-

red with Fig. 28 a). The propulsive efficiency of this propeller SR-4BL in cruise condition in dependence of blade loading is shown in Fig. 29 and in dependence of power loading in Fig. 30. With this propeller a propulsive efficiency between 79 % and 88 % is possible in the useful power range.

3.2.2 <u>Counter rotating propeller</u>

In the context of the present study the comparison of this propeller with two counter rotating propellers is of special interes, i. e. one with two two-bladed rotors of equal solidity (CR-2 + 2BL) and one with twice the solidity, where the original single rotating propeller is doubled (CR-4 + 4BL). The propulsive efficiency of all these propellers can be compared in Fig. 29 and 30. When the single and counter rotating propeller is compared at the same solidity and nearly the same power (points A and C in Fig. 29 and 30) an efficiency advantage for counter rotation of around 9 % is evident. This is in concordance with the trend in Fig. 25 /11/.

The propulsive efficiency of the counter rotating propeller with twice the solidity (CR-4 + 4BL) falls between the lines of the previously discussed propellers for a given blade loading, as can be seen in Fig. 29. This is due to the higher friction of twice the number of blades. But an advantage of 3 % to 5 % remains over single rotation. The advantage of the higher solidity propeller is clearly evident from Fig. 30 in that a much higher power can efficiently be absorbed.

For point D in Fig. 29 and 30 with the same blade angle of the first rotor as in point A (Fig. 28) the wake model and performance data are shown in three time steps in Fig. 31. The periodic change in thrust is from + 3 % to - 2,2 % and in power from + 3,5 % to - 2,5 % of the average values. For equal power the blade angle of the second rotor needs to be 2,5 deg. higher than that of the first rotor. The thrust of the second rotor is 86 % of the value of the first one. This example needs 12 sec computer time. For more time steps a corresponding increase in computer time is needed, but when only overall performance data are of interest only a few time steps are sufficient.

The corresponding results for point E in Fig. 29 and 30 are given in Fig. 32. This condition represents the highest power loading considered, where a propeller of only 1,85 m diameter absorbs around 1450 kW. The periodic change in thrust here is only + 1,3 % and in power + 1,2 % of the average values. So the more blades are used, the less vibration in thrust and power can be expected. In this case the computer time is 36 sec.

To explain the propulsive advantages of counter rotation over single rotation the points B and C in Fig. 29 and 30 with an efficiency difference of around 11 % and nearly equal power are compared in Fig. 33. The main reasons for this difference can be concluded from the distributions of the local lift coeffi-

cient (Fig. 33 a) and swirl angle (Fig. 33 b). The lift coefficients on the counter rotating rotors show relatively even distributions along the blades (Fig. 33 a) and the effective swirl angle is practically zero, whereas the single rotation propeller shows - for identical blade geometry - an unloading of the inner blade area and an increased loading of the blade tip area. This change in blade loading is due to the relatively constant swirl angle of 5 deg. (Fig. 33 b), which is the primary cause for the efficiency loss.

4.   OUTLOOK

As was shown by the different examples of fixed and oscillating wings, single and counter rotating rotors and propellers the described method proves to be an efficient tool for the design and perfomance calculation of counter rotating rotors and propellers. In the first design iterations and for the building up of performance charts relatively crude representations of the rotor blades can be utilized with good accuracy and relatively little computer time.

To improve the accuracy of the calculation method in the high loading hover case the introduction of a thrust dependent wake contraction for the first rotor is intended. The validation of the method has to be done for advancing single and counter rotating helicopter rotors with flapping and lagging blades.

Then the calculation of coaxial propellers in skewed flow (Fig. 34) and in non-uniform onset flow is of great importance for high speed propeller integration problems. Also an introduction of compressible actuator disk theory in the downwash correction calculation is intended for propellers operating at high subsonic cruise Mach number (Fig. 35).

5.   REFERENCES

/1/   A. Azuma, K. Kawachi, Local Momentum Theory and its Application to the Rotary Wing, J. Aircraft, Vol.16, No.1, Jan. 1979.

/2/   A. Azuma, S. Saito et al., Application of the Local Momentum Theory to the Aerodynamic Characteristics of Multi-Rotor-Systems, Vertica, Vol.3, No.2, 1979.

/3/   K. Kawachi, An Extension of the Local Momentum Theory to the Distorted Wake of a Hovering Rotor, NASA TM 81258, Feb. 1981.

/4/   A. Azuma, et al., An Extension of the Local Momentum Theory to the Rotors Operating in Twisted Flow Field, Paper presented at 7th European Rotorcraft Forum, Garmisch-Partenkirchen, Sept. 1981.

/5/   S. Saito, et al., A Numerical Approach to Co-Axial Rotor
        Aerodynamics, <u>Paper presented at 7th European Rotor-
        craft Forum,</u> Garmisch-Partenkirchen, Sept. 1981.

/6/   T. Nagashima, et al., Optimum Performance and Wake Geo-
        metry of Co-Axial Rotor in Hover, <u>Paper presented at
        7th European Rotorcraft Forum,</u> Garmisch-Partenkirchen,
        Sept. 1981.

/7/   M. J. Andrew, Co-Axial Rotor Aerodynamics in Hover, <u>Pa-
        per presented at 6th European Rotorcraft and Powered
        Lift Aircraft Forum,</u> Bristol, Sept. 1980.

/8/   C. du P. Donaldson, et al., Vortex Wakes of Conventional
        Aircraft, <u>AGARDograph No. 204,</u> 1975.

/9/   H. Zimmer, The Rotor in Axial Flow, Aerodynamics of Ro-
        tary Wings, <u>AGARD-CP-111,</u> 1972.

/10/   R. D. Harrington, Full-Scale-Tunnel Investigation of the
        Static-Thrust Performance of a Coaxial Helicopter Ro-
        tor, <u>NACA TN 2318,</u> 1951.

/11/   D. C. Mikkelson, et al., Summary of Recent NASA Propel-
        ler Research, <u>AGARD-CP-366,</u> 1984

/12/   H. Zimmer et al., Investigation of Modern General Avia-
        tion Propellers, <u>AGARD-CP-366,</u> 1984.

/13/   K. H. Horstmann, et al., Entwicklung von vier Profilen
        für einen Experimentalpropeller in der Leistungsklasse
        750 PS, <u>Paper presented at the annual meeting of DGLR,</u>
        Stuttgart, 1982.

FIG. 1: Coaxial Rotor Configurations
of interest:

a) Helicopter like Surveillance
System
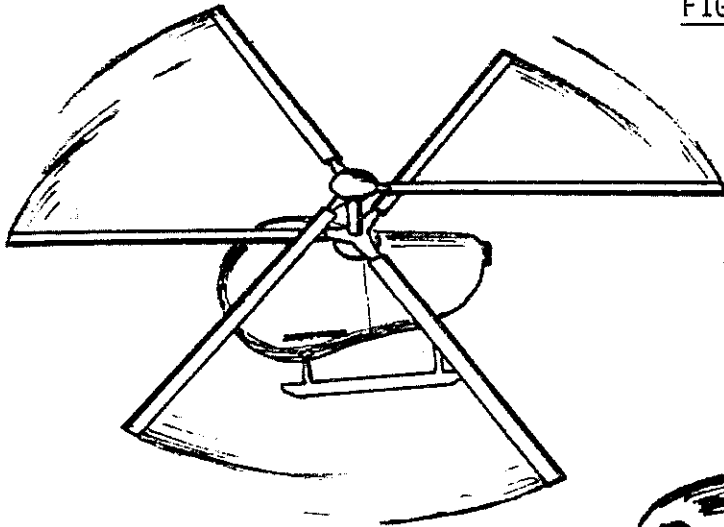
b) Counter rotating Propfan

(GE UDF TM)
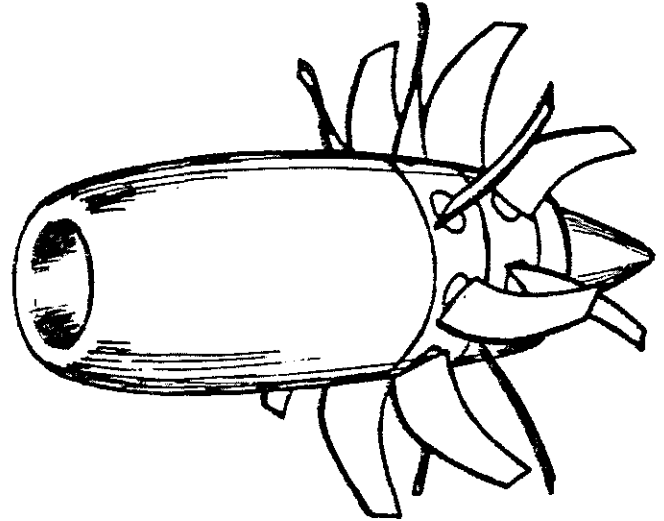
——— : Local Momentum Theory (One-Sided)
—·—· : Local Momentum Theory (Symmetric)
——— : Lifting Line Theory by Multhopp
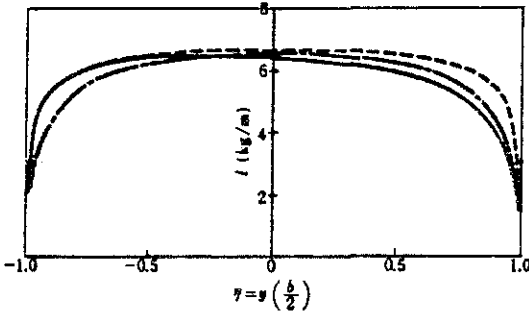
a) Lift distribution
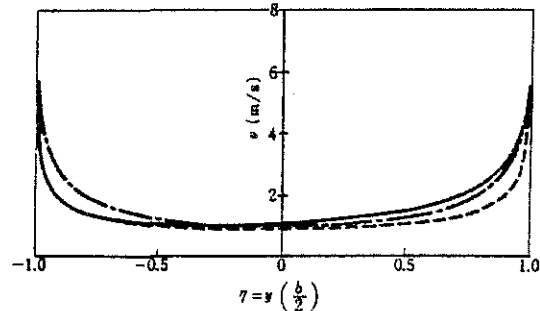
b) Induced velocity distribution

FIG. 2: Lift and induced velocity distributions for a
rectangular wing (AR = 6, n = 50) [1]
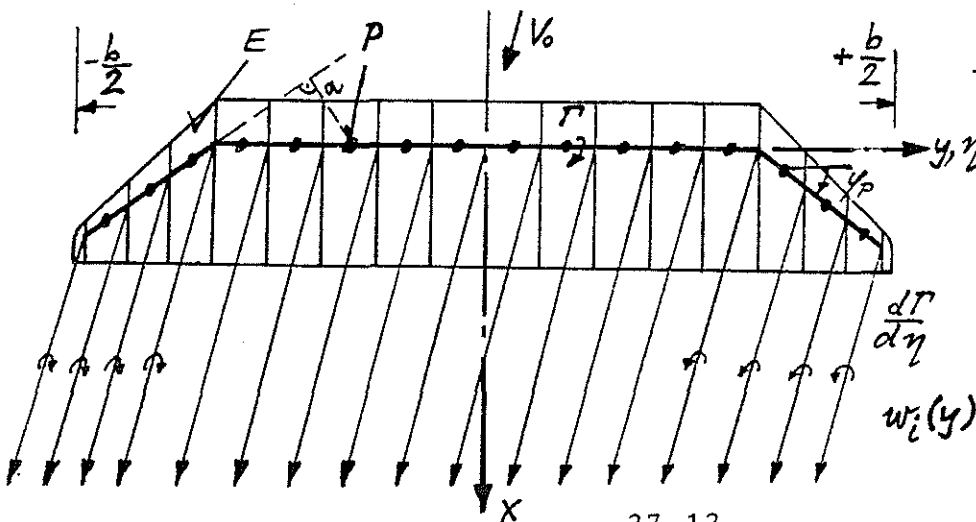
FIG. 3: Representation
of a wing

$$w_i(y) = \frac{1}{4\pi} \int_{-\frac{b}{2}}^{\frac{b}{2}} \left(\frac{d\Gamma}{d\eta} + \frac{\Gamma(y)}{\alpha(y)} \right) \frac{d\eta}{y - \eta}$$

27-12
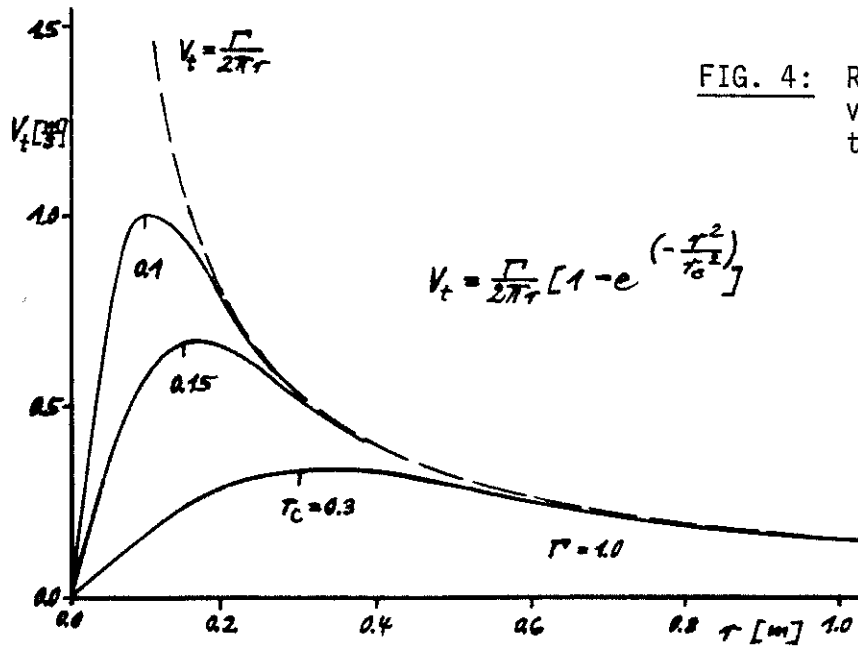
FIG. 4: Representation of all vortices according to the LAMB-Vortex-Concept

$$V_t = \frac{\Gamma}{2\pi r}\left[1 - e^{\left(-\frac{r^2}{r_0^2}\right)}\right]$$

$\Lambda = 5.0$
$\alpha = 0.1$

	n	C_l	C_{di}
▼	11	0.4208	0.0118
△	21	0.4253	0.0120
O	41	0.4419	0.0122
——	MULTHOPP		
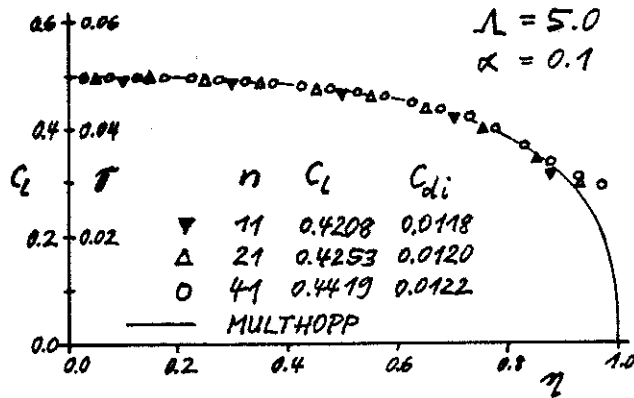
FIG. 5: Comparison of a calculated rectangular wing with MULTHOPP-Theory

$\Lambda = 7.05$

	n	C_l	C_{di}
▲	17	0.803	0.0272
O	25	0.797	0.0276
——		0.7853	0.02722

▲	O	PRES. CALC.
——		VORTEX LATTICE
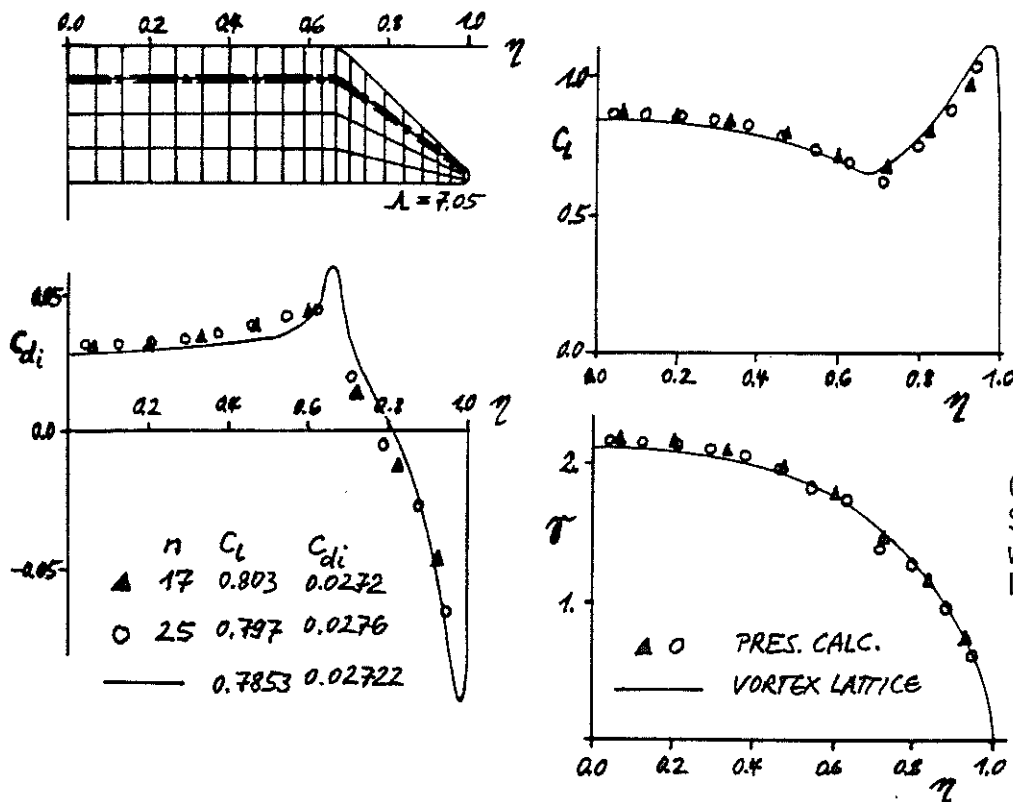
FIG. 6:

Comparison of a Swept tip wing with Vortex-Lattice Theory

a)

b)

$$w_\xi = \frac{H}{2}\,\omega \cdot \cos\psi$$

$$V_{RF} = \sqrt{V^2 + w_\xi^2}$$

$$\varepsilon = \arctan \frac{w_\xi}{V}$$

c)
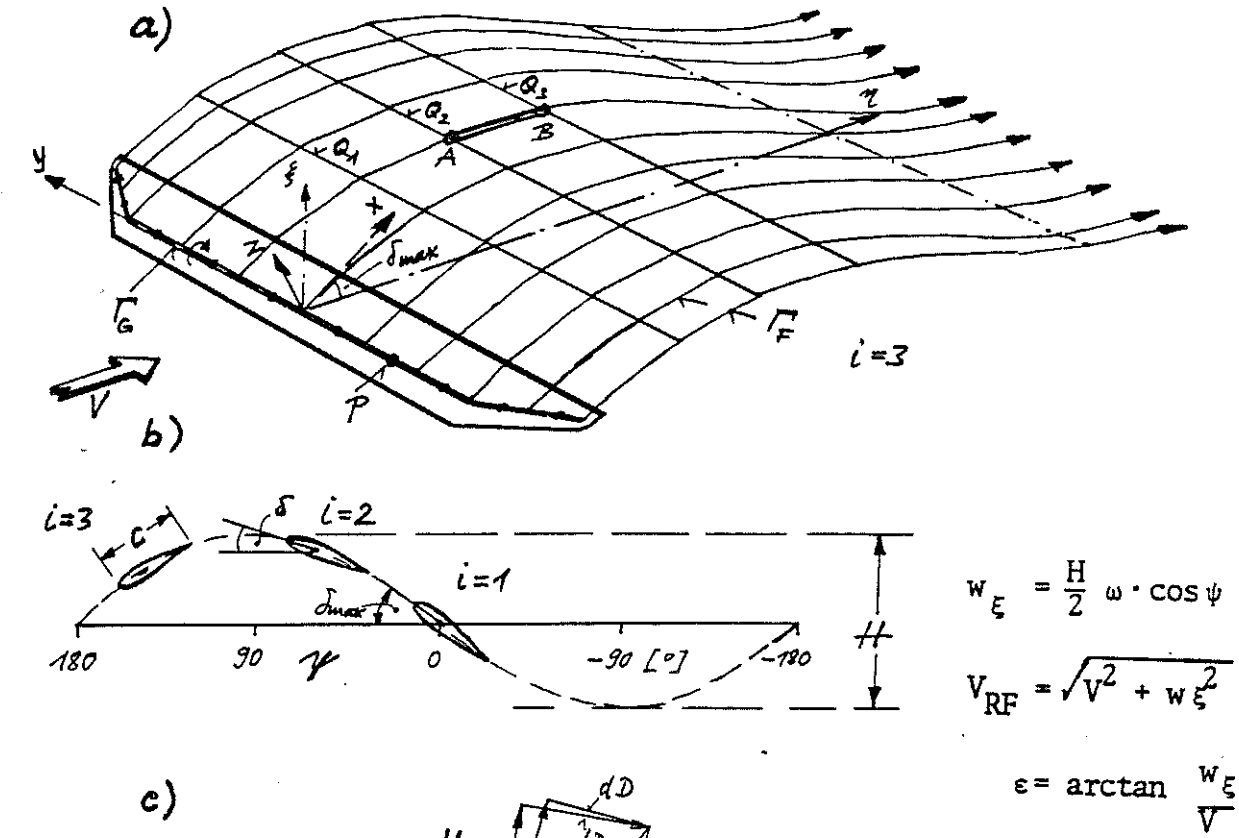
FIG. 7: Representation of an oscillating wing

FIG. 8: Comparison of oscillating wing results with 2D-Flutter Theory

$$c_P' = \frac{P}{\frac{\rho}{2} V_o^3 \, H \cdot b}$$

$\Lambda = 5.95$

$\frac{dc_L}{d\alpha} = 4.696$

$a = \frac{\hat{\delta}_{max}}{H/c} = 0.3$

——— 2D-FLUTTER THEORY ($dC_L/d\alpha = 4.696$)
——— QUASI STATIONARY WAKE
— — NONSTATIONARY WAKE (1÷3 SHED VORTICES)

$\bar{\omega} = \frac{\omega \cdot c}{V_o}$
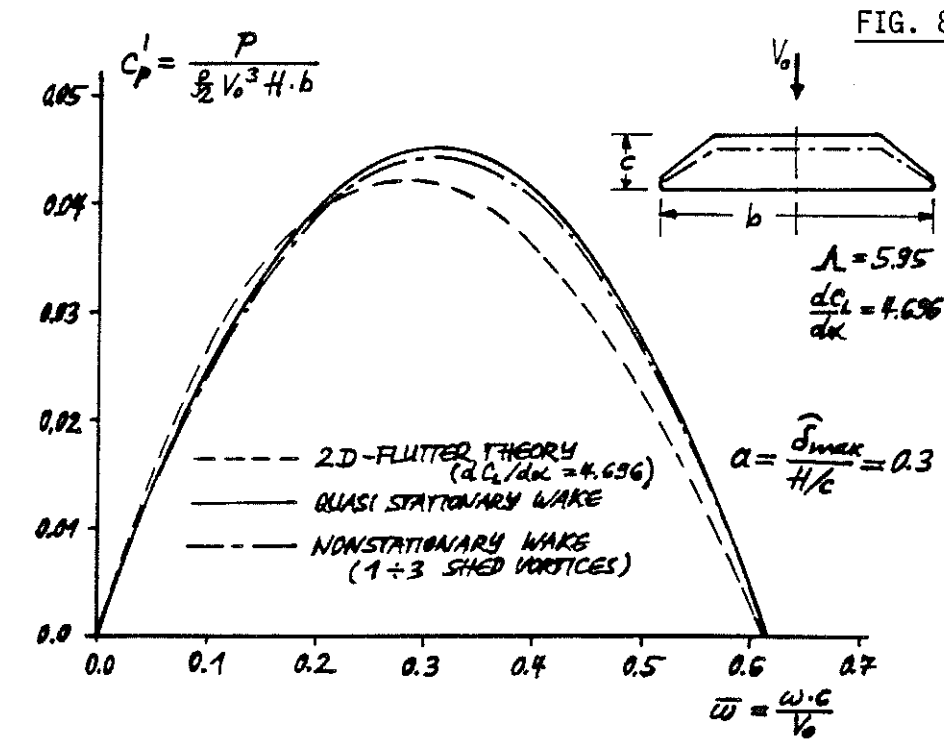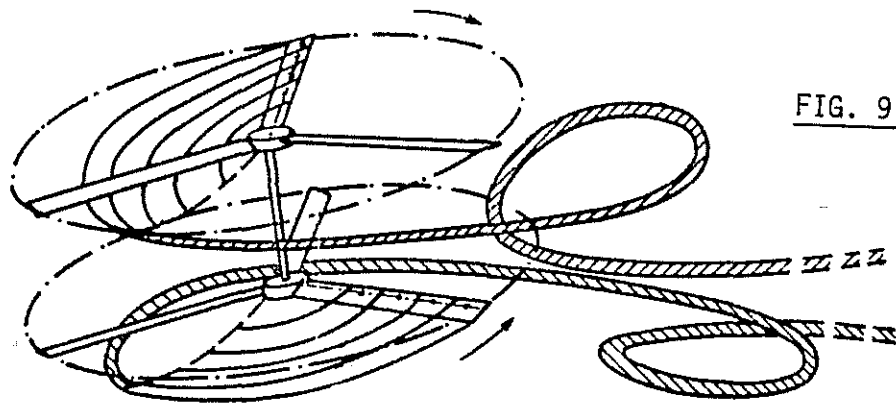
FIG. 9: Blade wakes of a Coaxial Rotor Schematic

STEP $i = 1$
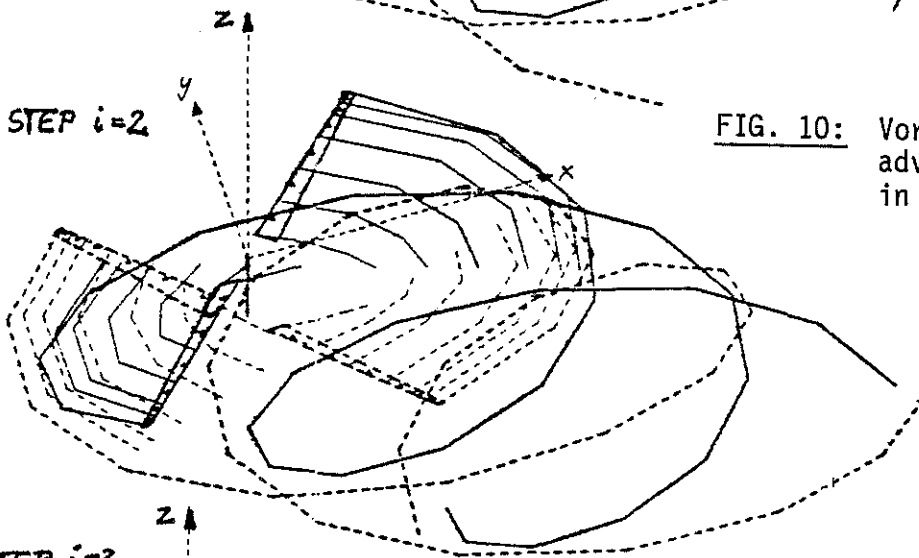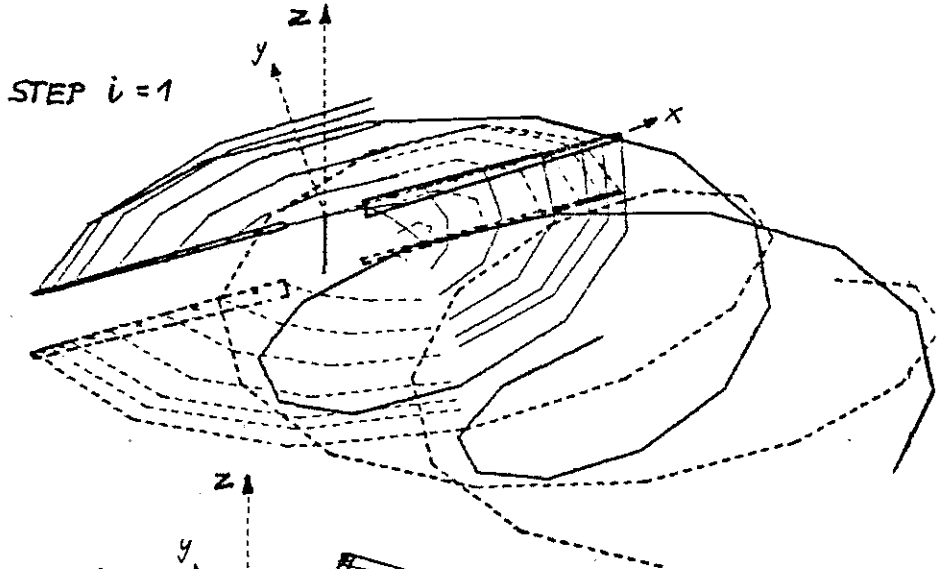
FIG. 10: Vortex wake model of an advancing Coaxial Rotor in 3 time steps

STEP $i = 2$

STEP $i = 3$

a)

b)

$$dL = C_L \frac{\rho}{2} c\, V_R^2\, dr$$

$$dD = C_D \frac{\rho}{2} c\, V_R^2\, dr$$

$$dT = \frac{\rho}{2} c\, V_R^2 [C_L \cos(\alpha_i + \delta) - C_D \sin(\alpha_i + \delta)]\, dr$$

$$dM_Q = \frac{\rho}{2} c\, V_R^2 [C_L \sin(\alpha_i + \delta) + C_D \cos(\alpha_i + \delta)]\, r\, dr$$
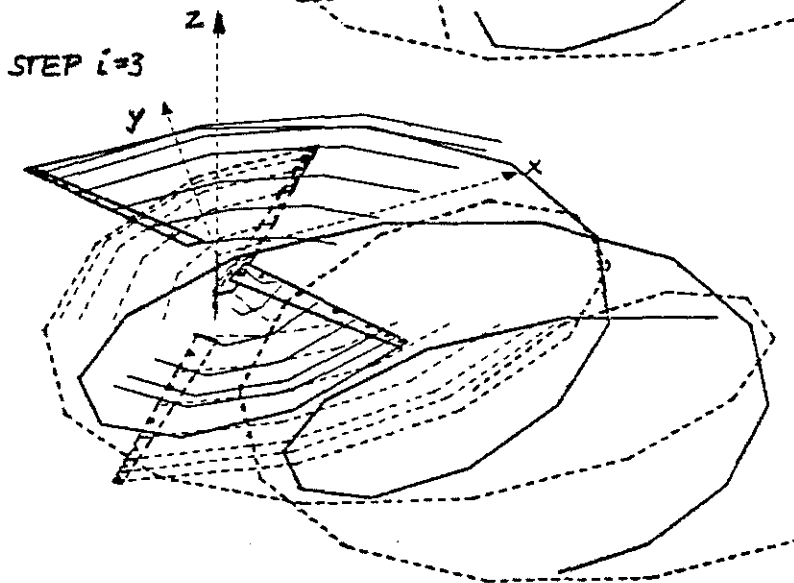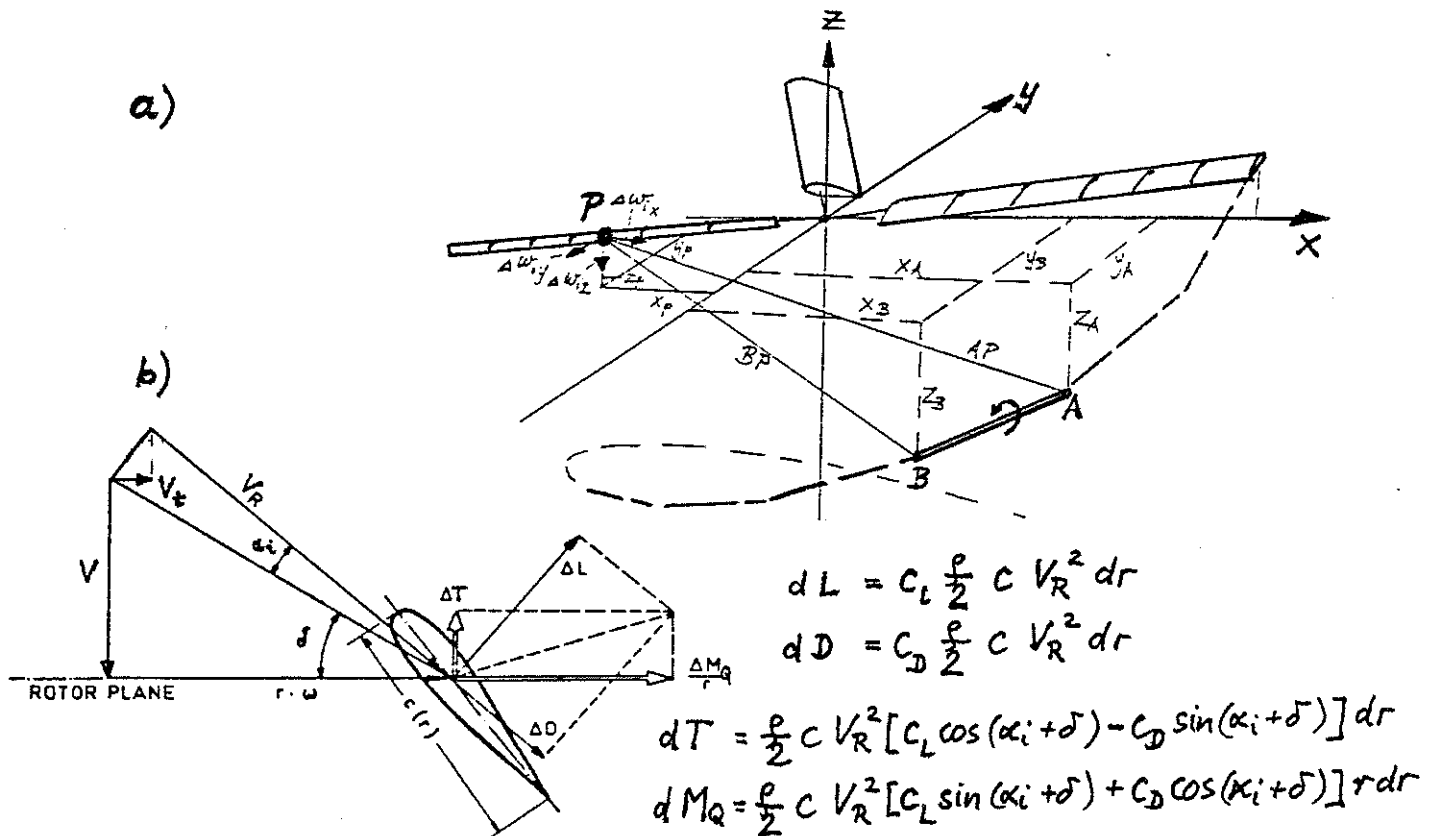
$$V_t = \frac{dM_Q}{d\dot{m} \cdot r}$$

c)

$$T_i = \int_{ROTOR\,1,2} \int_0^{2\pi} \int_0^R dT\, dr\, d\psi$$

$$M_{Q_i} = \int_{ROTOR\,1,2} \int_0^{2\pi} \int_0^R dM_Q\, dr\, d\psi$$

$$L_i = \int_{ROTOR\,1,2} \int_0^{2\pi} \int_0^R dT\, r\sin\psi\, dr\, d\psi$$

$$M_i = \int_{ROTOR\,1,2} \int_0^{2\pi} \int_0^R dT\, r\cos\psi\, dr\, d\psi$$

d)

INPUT:

ROTOR GEOMETRY
WORKING CONDITIONS
GEOMETRY OF TIP VORTEX
LENGTH OF BLADE WAKE
    UP TO ROLLING UP
PARAMETERS DEFINING
BLADE PROFILE AERODYNAMICS

LIFT DISTRIBUTION
$\Delta T = \frac{\rho}{2} c\, V_R^2 [c_L \cos(\alpha_i + \delta) - c_D \sin(\alpha_i + \delta)] \Delta r$
BOUND CIRCULATION
FREE CIRCULATION
DOWNWASH CORRECTION

WAKE MODELL (FIG. 10)
TIP VORTEX AND RADIAL POSITION OF
VORTICES IN BLADE WAKE ARE KNOWN
AXIAL DISPLACEMENT OF BLADE WAKE
ACCORDING TO INDUCED DOWNWASH

NEW DISTRIBUTION OF INDUCED
ANGLE OF ATTACK α_i

α_i CONVERGES

NO

YES

ROTOR THRUST AND MOMENT

FIG. 11: Calculation Procedure in every Time Step

27-16

FIG. 12:

a) b) Mutual Rotor
Interference

c) Downwash
Correction

d) Computation of
Rotor Forces
and Moments
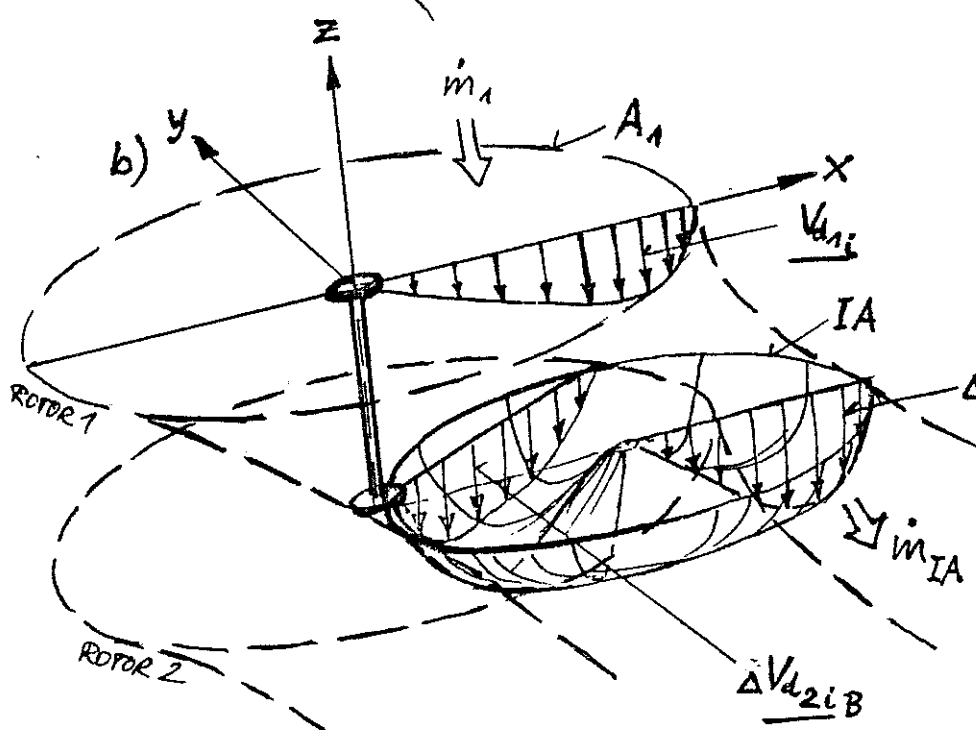
$$\Delta V_{d_{2i}} = \frac{A_1}{IA} \cdot V_{d_1 i}$$

$$\dot{m}_1 = \dot{m}_{IA}$$
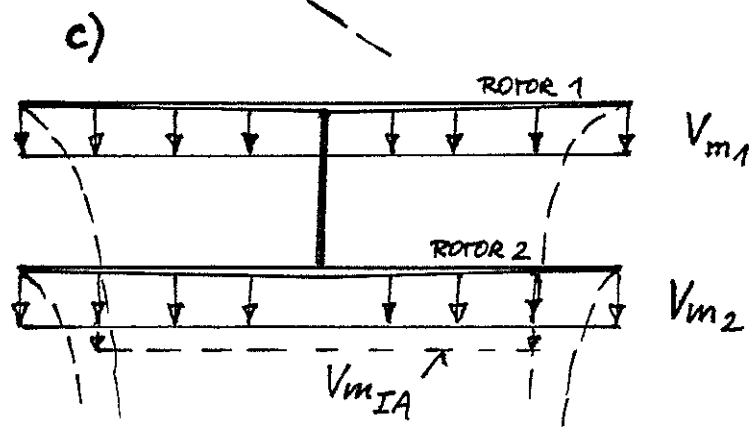
$$V_{mx} = \frac{V_{m_1} + V_{m_2}}{2}$$

$$V_{mx_0} = \frac{V_z}{2} + \sqrt{\left(\frac{V_z}{2}\right)^2 + \frac{T_i}{2\rho A_1}}$$

$$V_{d_{1,2}i}\Big|_{cor.} = V_{d_{1,2}i} \frac{V_{mx_0}}{V_{mx}}$$

$$c_T^\bullet = \frac{1}{\rho \pi \Omega^2 R^4} \cdot \frac{1}{i} \sum_i T_i \qquad\qquad C_L = \frac{1}{\rho \pi \Omega^2 R^5} \cdot \frac{1}{i} \sum_i L_i$$

$$C_Q = \frac{1}{\rho \pi \Omega^2 R^5} \cdot \frac{1}{i} \sum_i M_{Qi} \qquad\qquad C_M = \frac{1}{\rho \pi \Omega^2 R^5} \cdot \frac{1}{i} \sum_i M_i$$
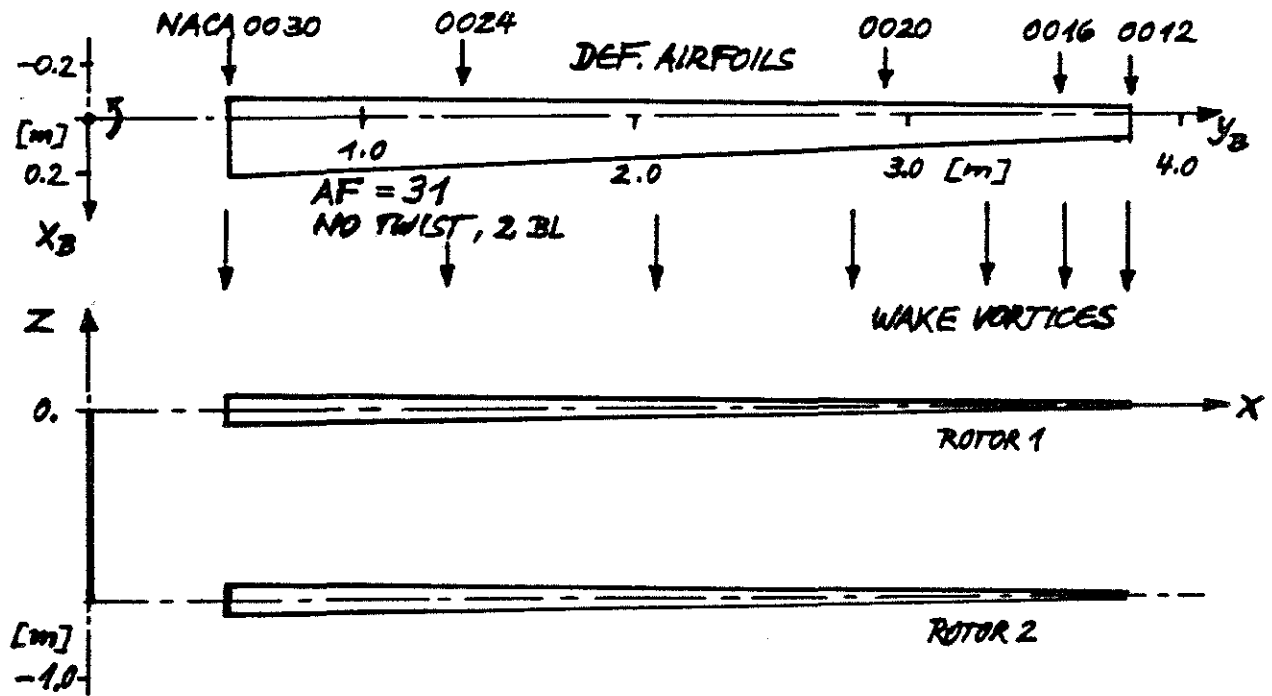
FIG. 13: Geometry of the Calculated Coaxial
Helicopter Rotor [10]
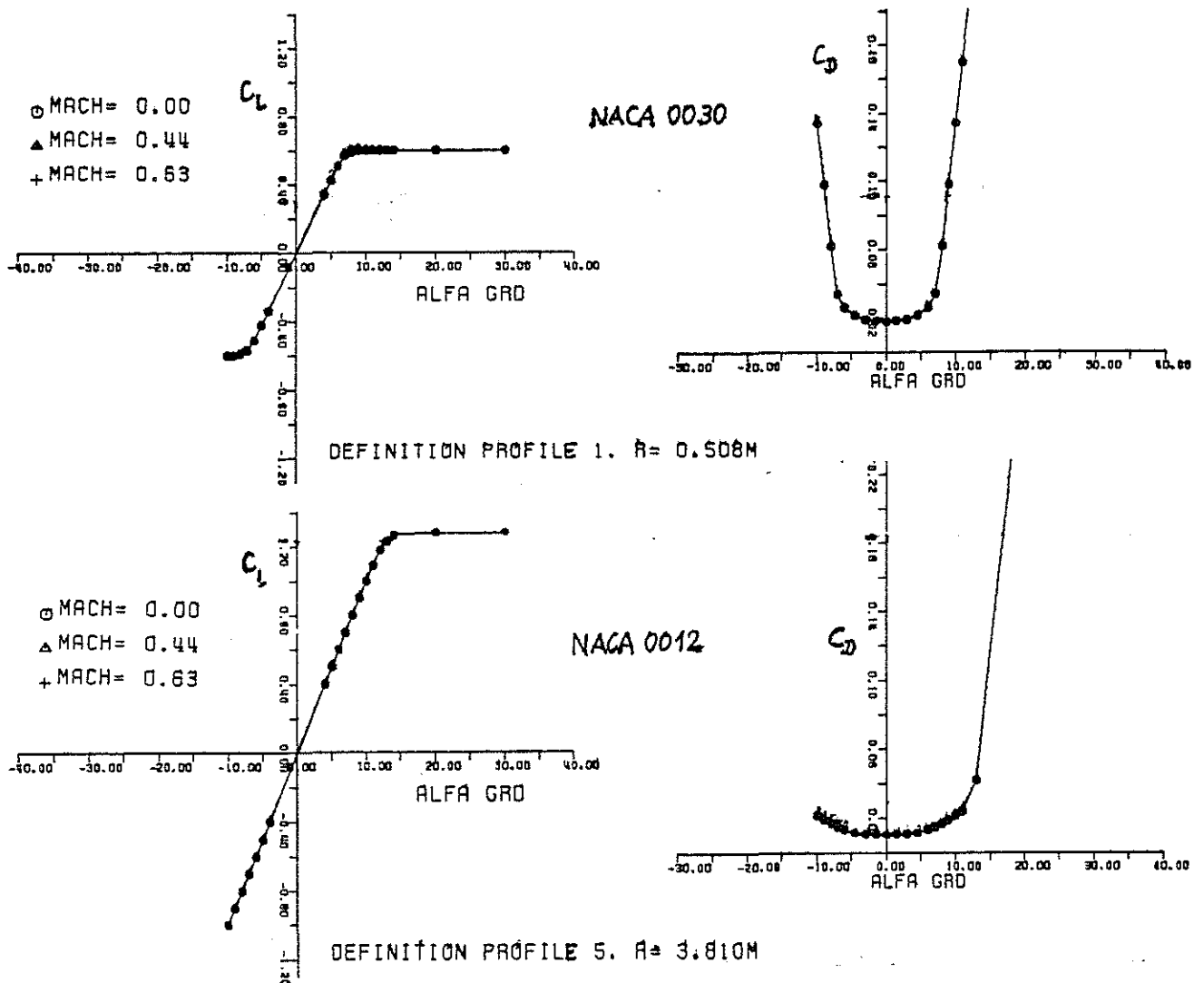
FIG. 14: Aerodynamic Characteristics of two Definition Airfoils
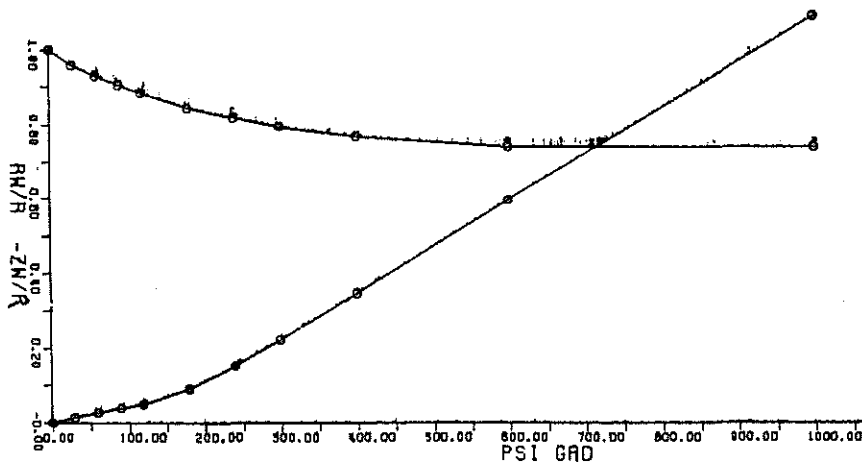
FIG. 15: Definition of the Tip Vortex for the Single Rotation Upper Rotor
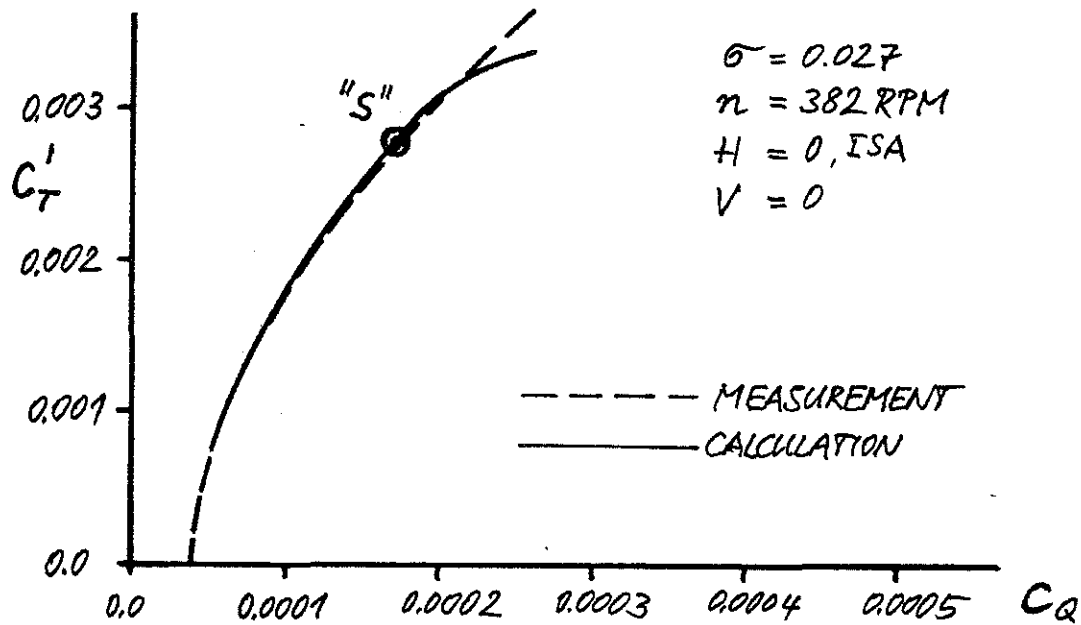
$\sigma = 0.027$
$n = 382 \, RPM$
$H = 0, ISA$
$V = 0$

— — — — — MEASUREMENT
———————— CALCULATION

FIG. 16: Comparison of the calculated and measured Performance

$\sigma = 0.027$
$n = 382 \, RPM$
$H = 0, ISA$
$V = 0$

— — — — — MEASUREMENT
———————— CALCULATION

FIG. 17: Comparison of the calculated and measured Hover Efficiency

"S": $\vartheta_{75} = 10°$
$n = 382\ RPM$
$H = 0, ISA, V=0$
$\sigma = 0.027$
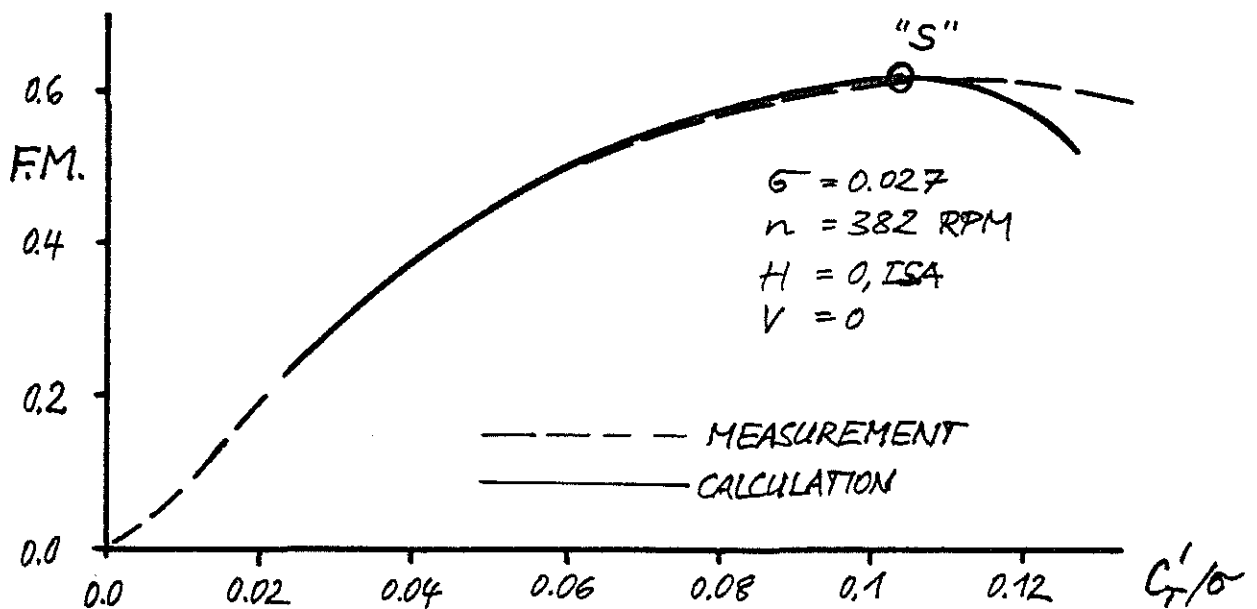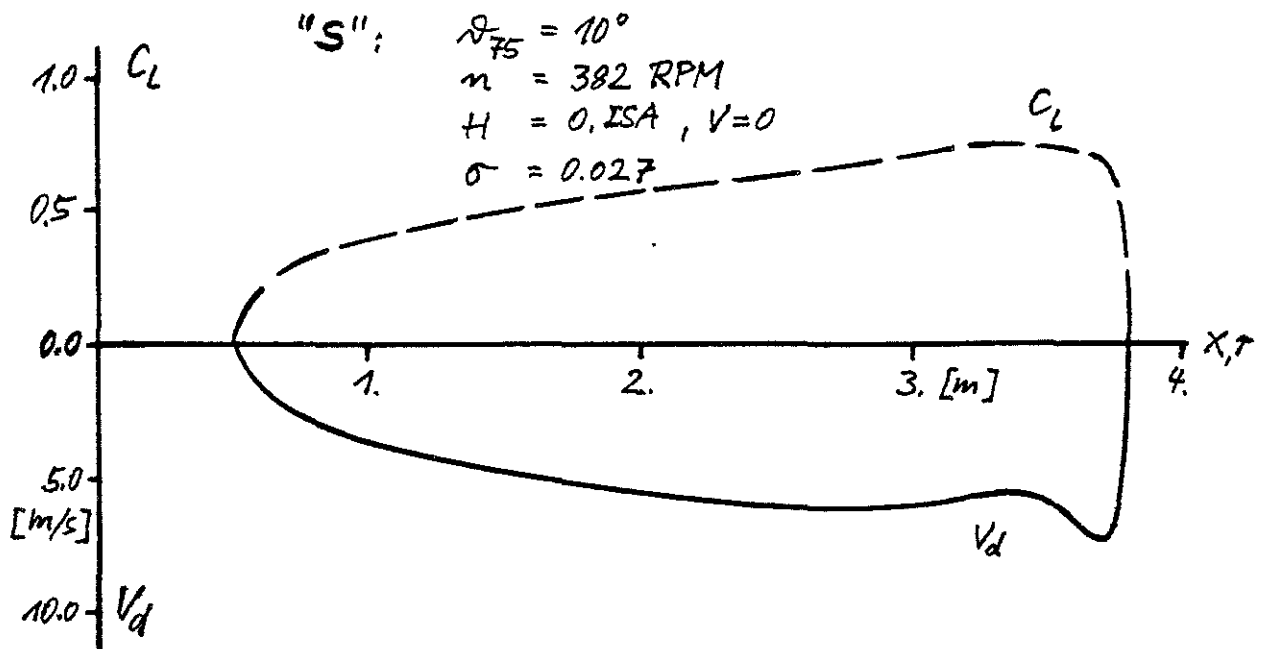
FIG. 18: Lift and Downwash Distribution in Point "S"

FIG. 19: Wake Model in Point "S"

"S": $\vartheta_{75} = 10°$
$n = 382\ RPM$
$H = 0, ISA, V=0$
$\sigma = 0.027$

$C_T' = 0.002793$

$C_T'/\sigma = 0.10344$

$C_Q = 0.000169$

$F.M. = 0.6170$

$(2.0\ S.\ CPU)$

27-20
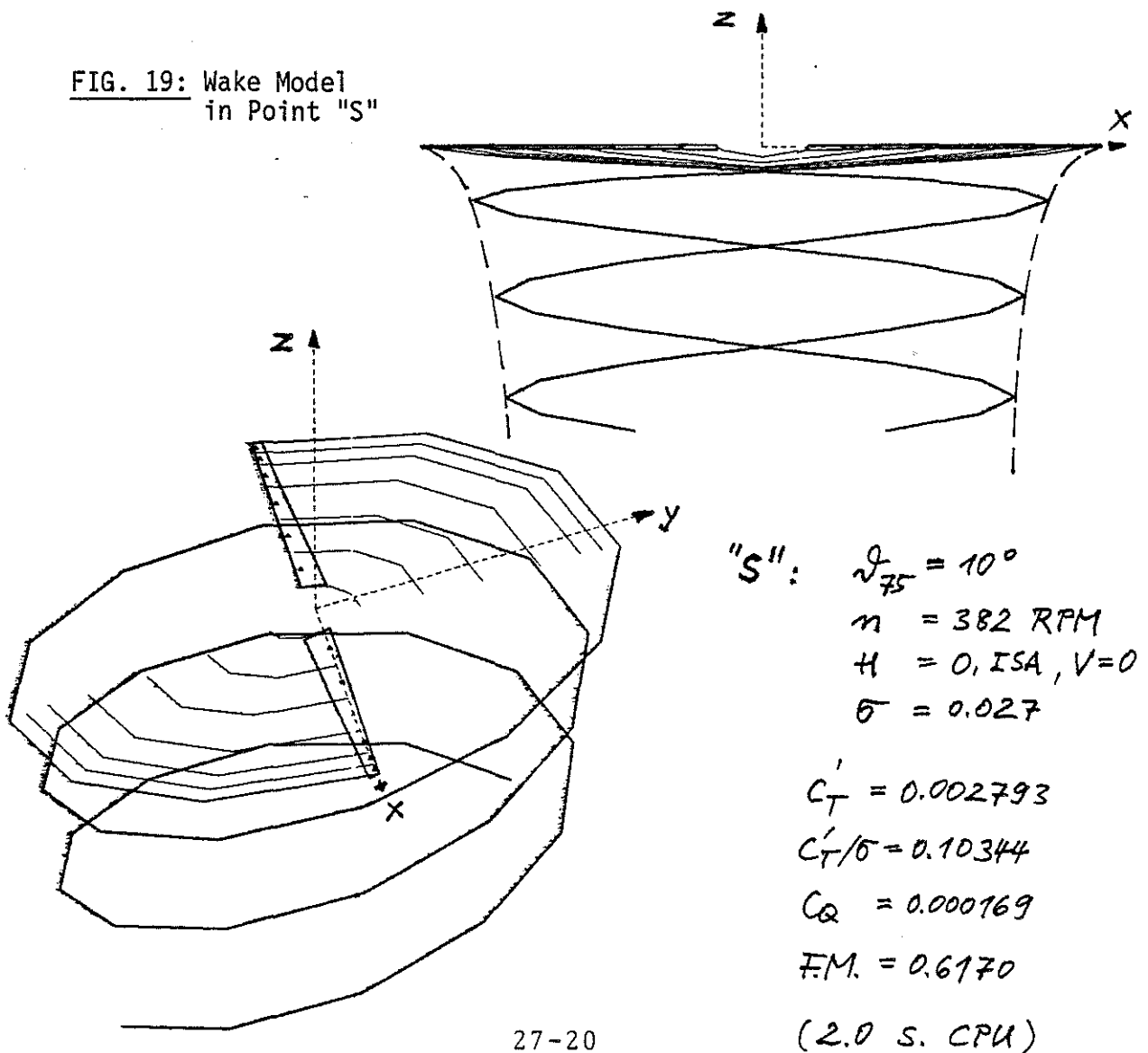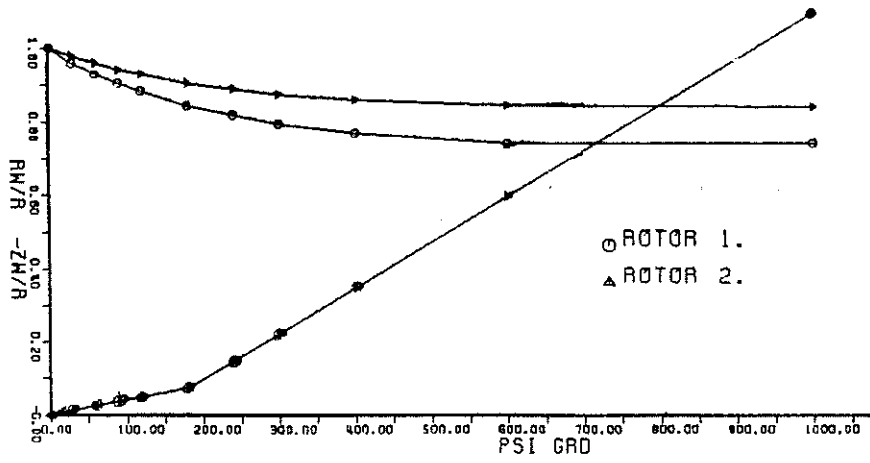
FULL-SCALE-COAXIAL-HELICOPTER-ROTOR ACC NACA TN 2318

FIG. 20: Definition of the Tip Vortices for the Coaxial Rotor

$\sigma = 0.054$

$n = 382$ RPM

$H = 0, ISA, V=0$

$P_2/P_1 \approx 1.0$

- - - - - MEASUREMENT
———— CALCULATION
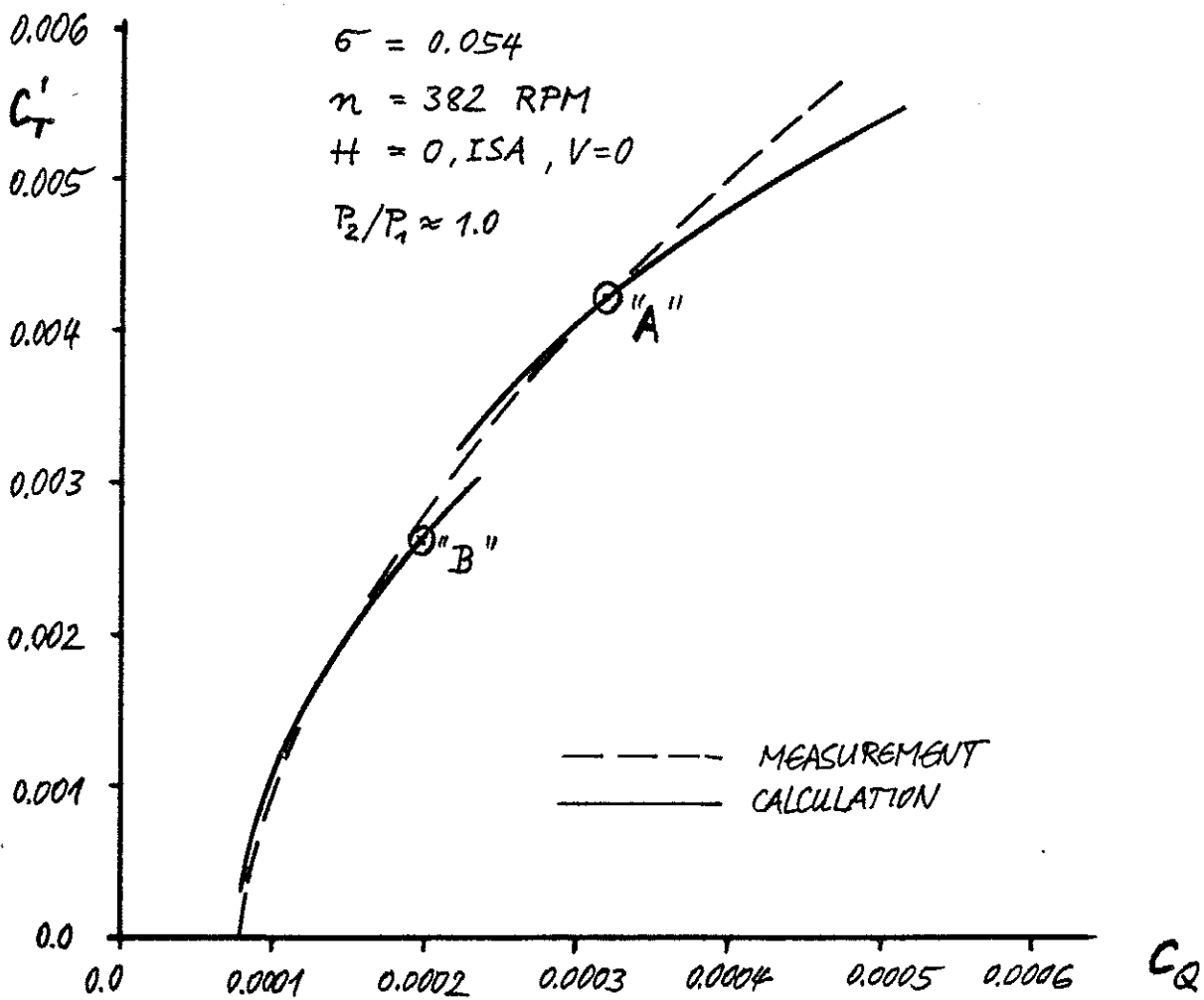
FIG. 21: Comparison of the calculated and measured Performance

27-21

FIG. 22: Comparison of the calculated and measured Hover Efficiency

Details from figure:

$\bar{\sigma} = 0.054$
$n = 382\ RPM$
$H = 0, ISA, V = 0$
$P_2/P_1 \approx 1.0$

$\dfrac{\dot{m}_1}{\dot{m}_{IA}} = 0.6$

$\dfrac{\dot{m}_1}{\dot{m}_{IA}} = 1.0$

– – – – MEASUREMENT
——— CALCULATION

$C_T'/\bar{\sigma}$

"A": $\vartheta_{75} = 10/12°$
$n = 382\ RPM, V = 0$
$H = 0, ISA$
$\bar{\sigma} = 0.054$

$C_T' = 0.004273$
$C_T'/\bar{\sigma} = 0.0791$
$C_Q = 0.000323$

$F.M. = 0.6108$
$P_2/P_1 = 0.95$
$T_2/T_1 = 0.81$
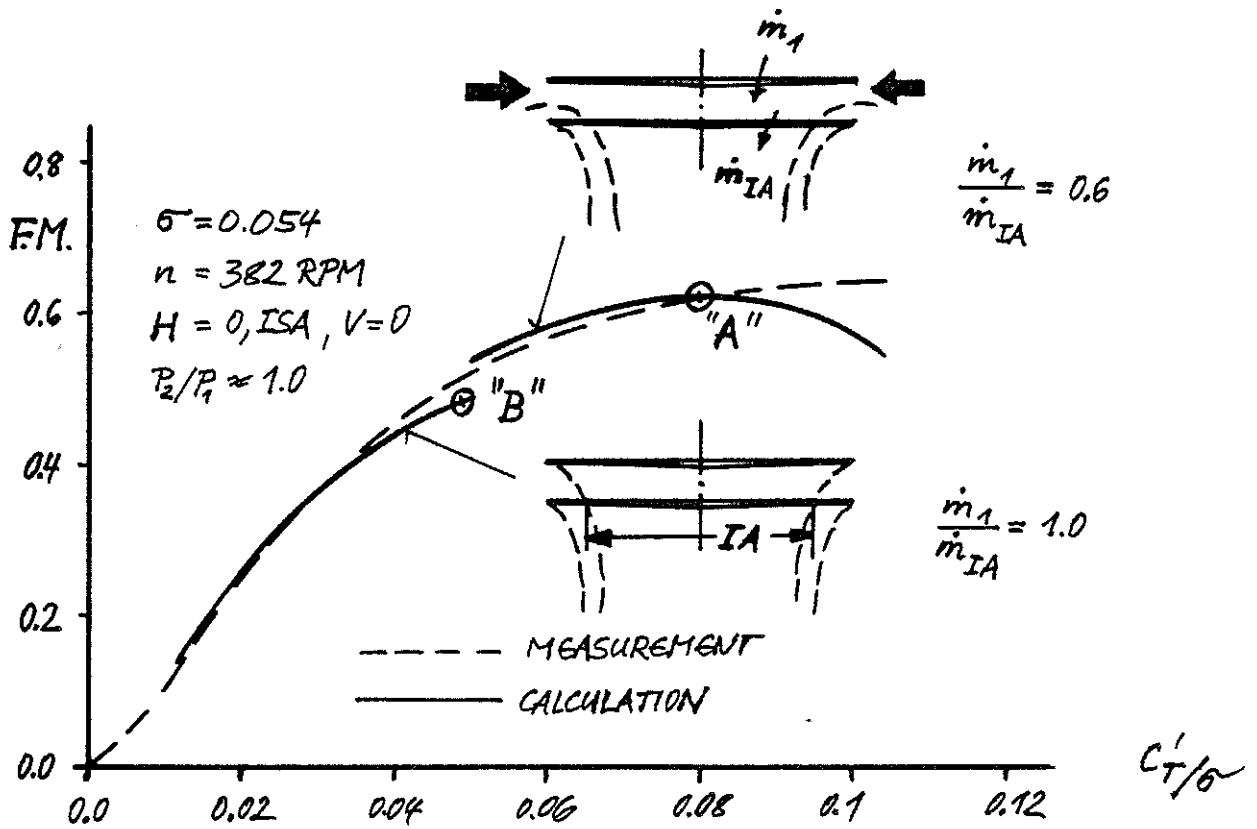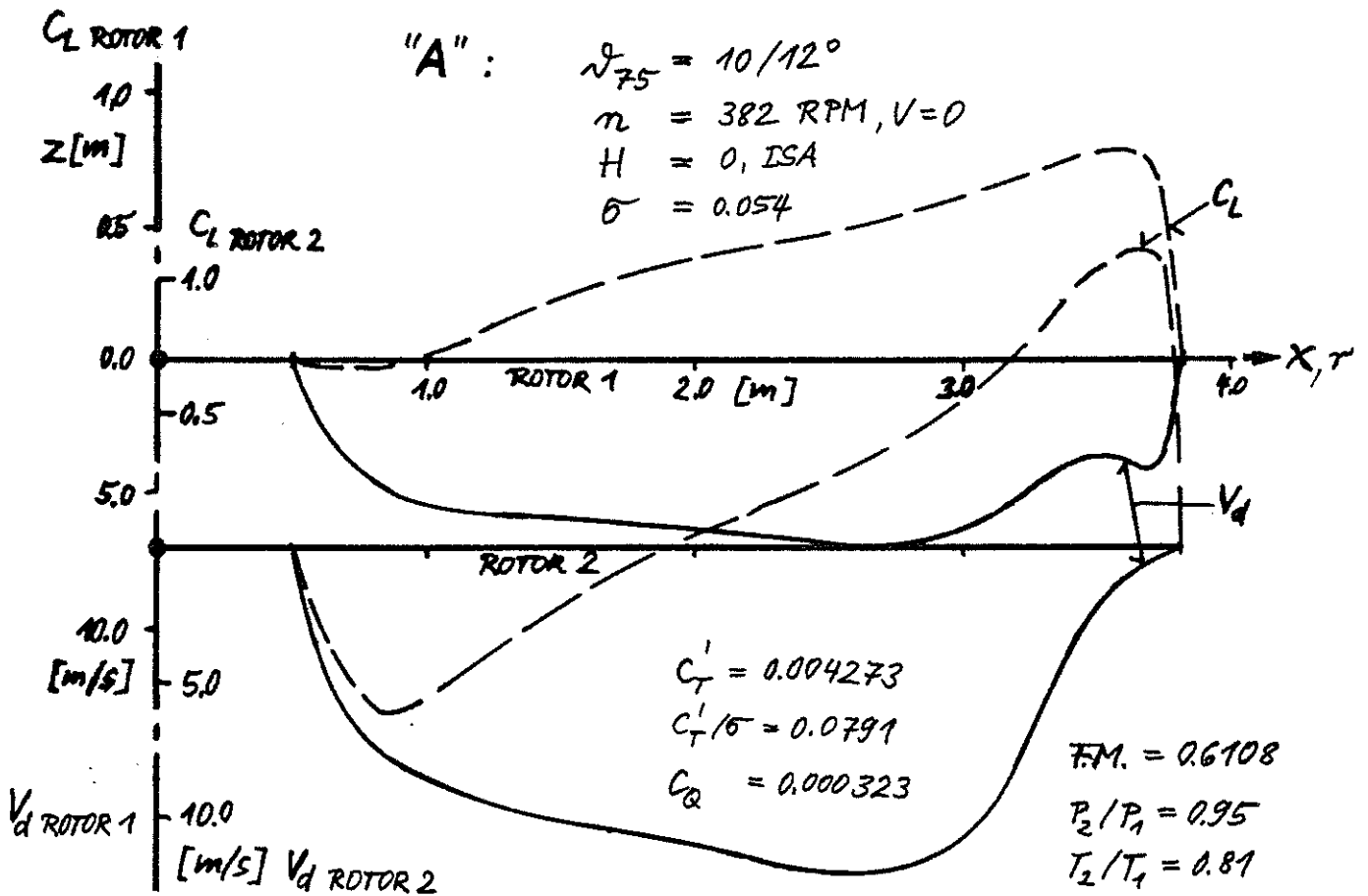
FIG. 23: Lift and Downwash Distributions in Point "A"

27-22

FIG. 24:

Wake Model in Point
"B" for 3 Time Steps

a)

b)

$"B"$: $\vartheta_{75} = 8/8.5°$

$n = 382\ RPM$

$H = 0, ISA, V=0$

$\sigma = 0.054$

$C_T' = 0.00261$

$C_Q = 0.000198$

$F.M. = 0.47592$

STEP 1:

$C_{T_1}' = 0.02637$

$C_{Q_1} = 0.000201$

STEP 2:

$C_{T_2}' = 0.002575$

$C_{Q_2} = 0.000191$

STEP 3:

$C_{T_3}' = 0.002617$

$C_{Q_3} = 0.000203$

$(12.2\ s.\ CPU)$

27-23
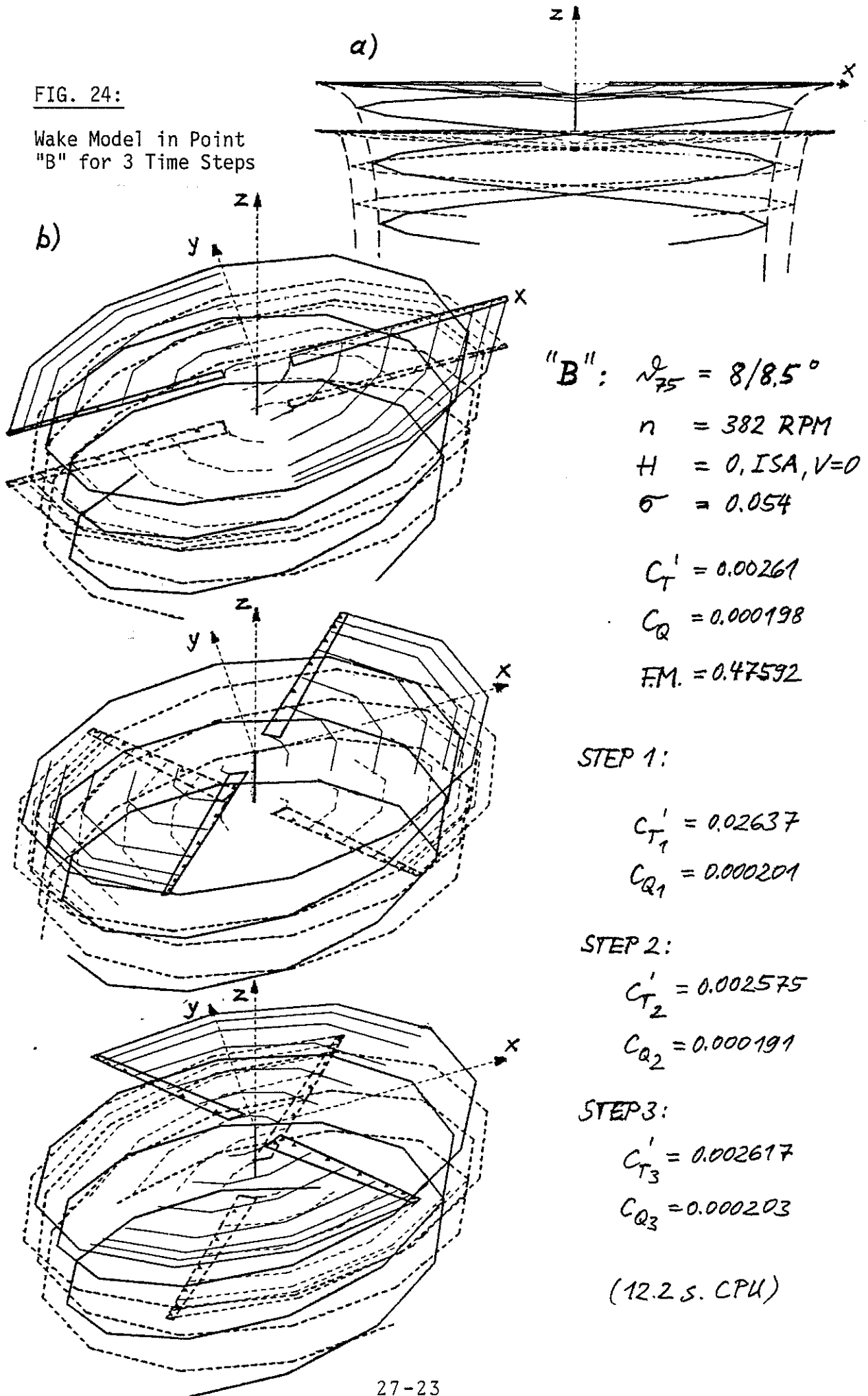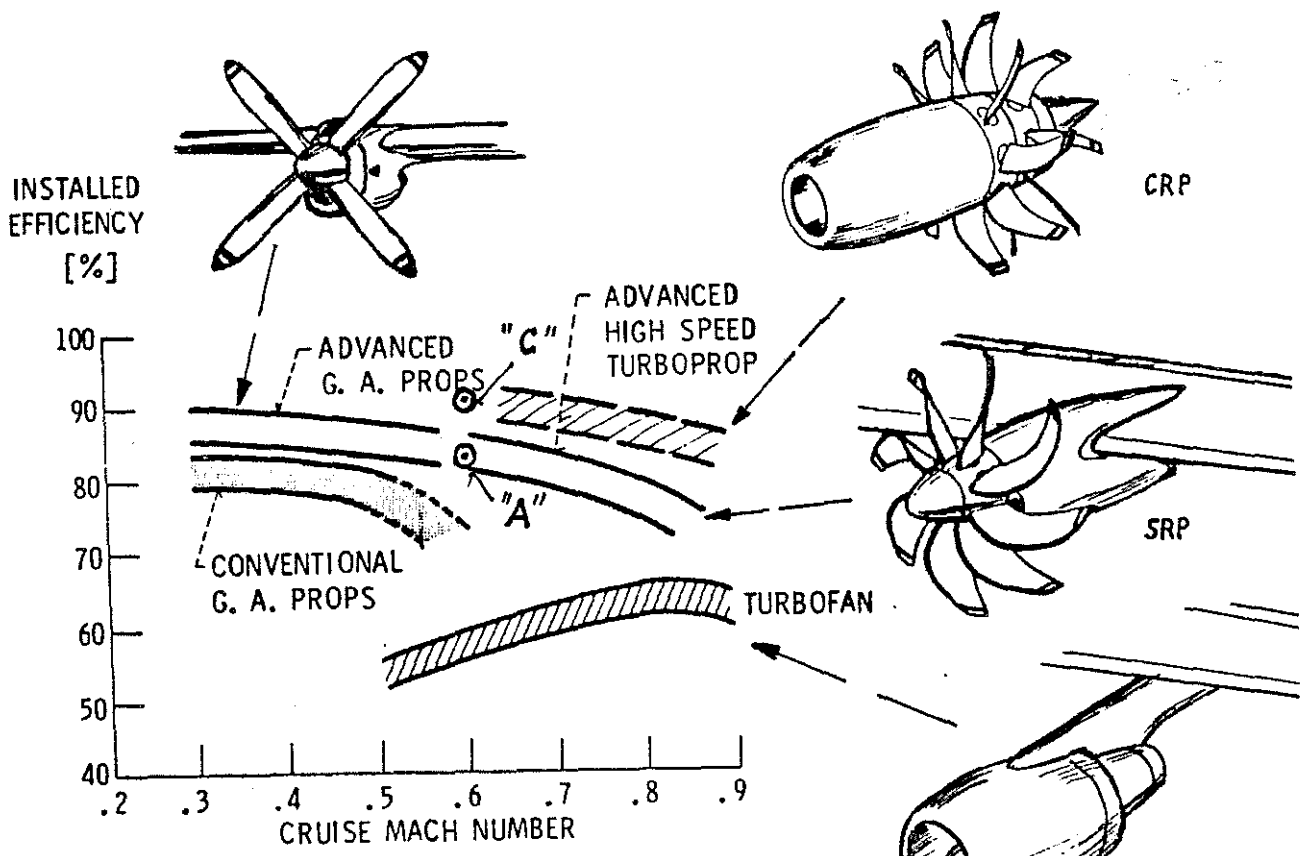
FIG. 25: Installed Cruise Efficiency Trends   [11]
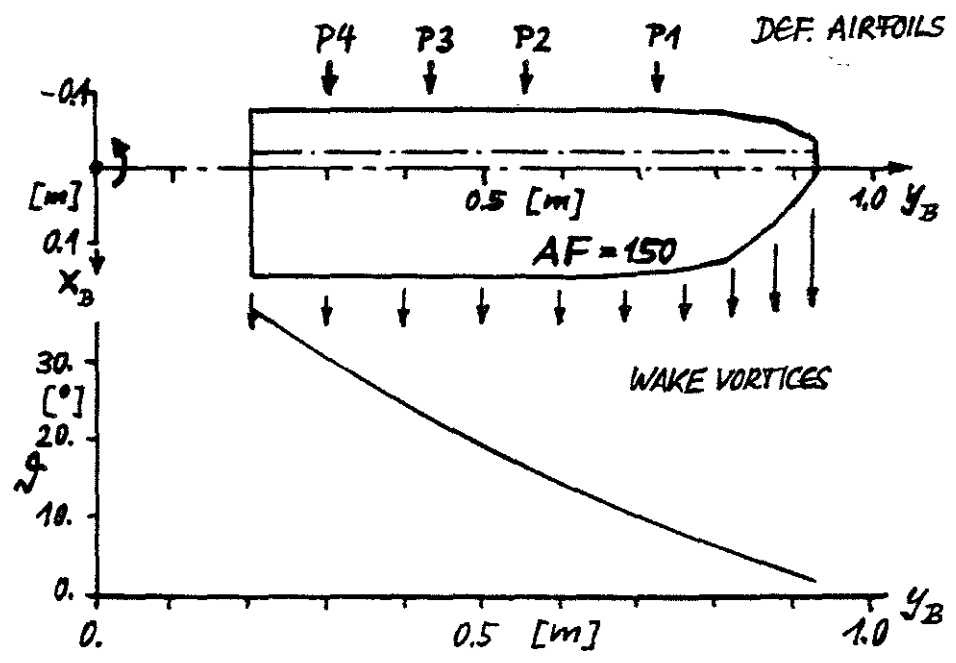
FIG. 26: Blade Definition of an Advanced G. A. Propeller
          for M = 0.6 Cruise Flight

Legend (upper left of first plot):
- ⊙ MACH= 0.15
- ▲ MACH= 0.50
- + MACH= 0.60
- × MACH= 0.70
- ◇ MACH= 0.80
- ▲ MACH= 0.90
- × MACH= 0.95

P1
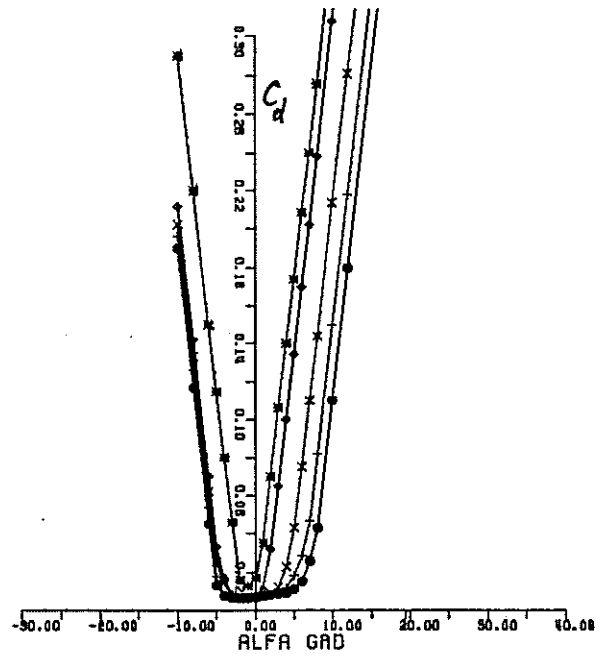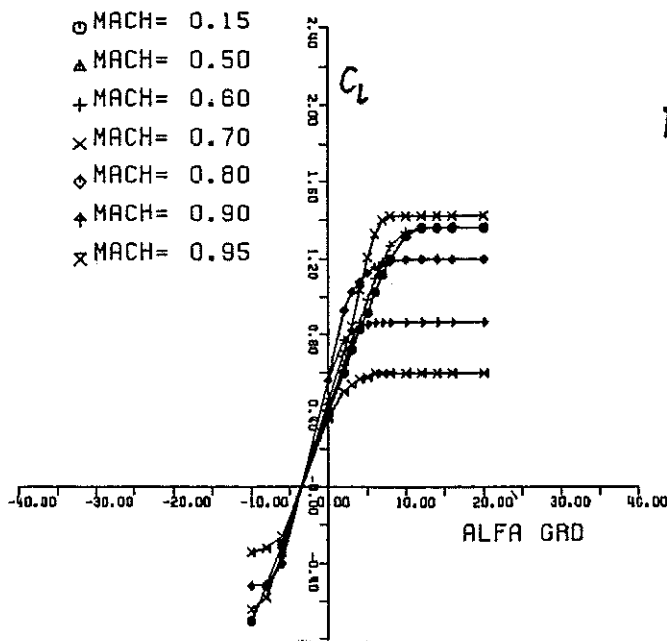
FIG. 27: Aerodynamic Characteristics at 0,725 m Radius

FIG. 28: Influence of Discretisation in Cruise Condition
(Point "A" in Fig. 25, SR-4BL)
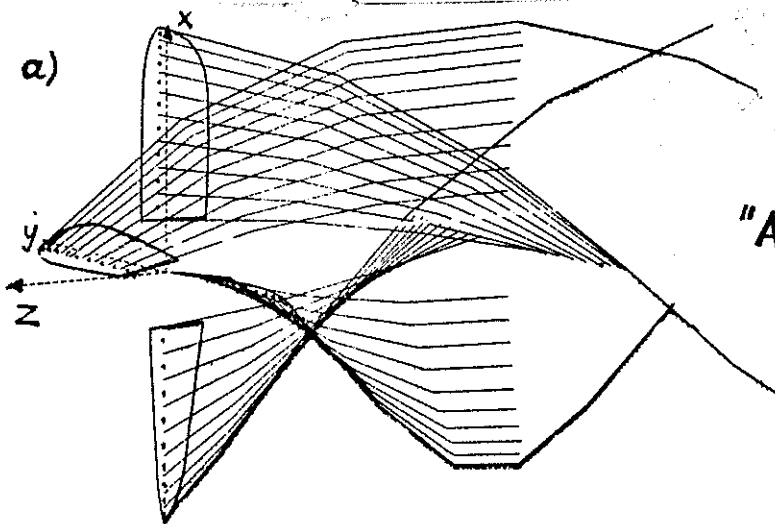
"A": $M = 0.6$
$H = 20000\ ft,\ ISA$
$n = 2133\ RPM,\ \vartheta_{75} = 53°$

$C_P = 0.7484$

$C_T = 0.2267$

$\eta_v = 0.8291$

(9.7 sec. CPU)
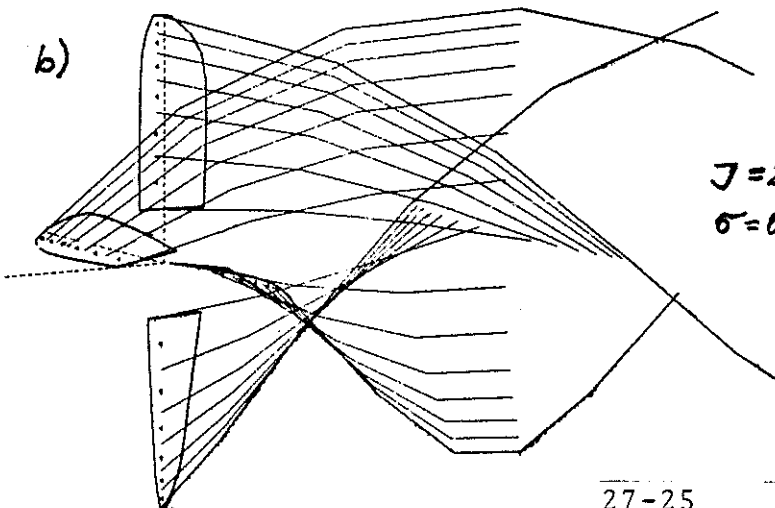
$J = 2.74$
$\sigma = 0.301$

$C_P = 0.7470$

$C_T = 0.2264$

$\eta_v = 0.8295$

(5.6 s. CPU)

27-25
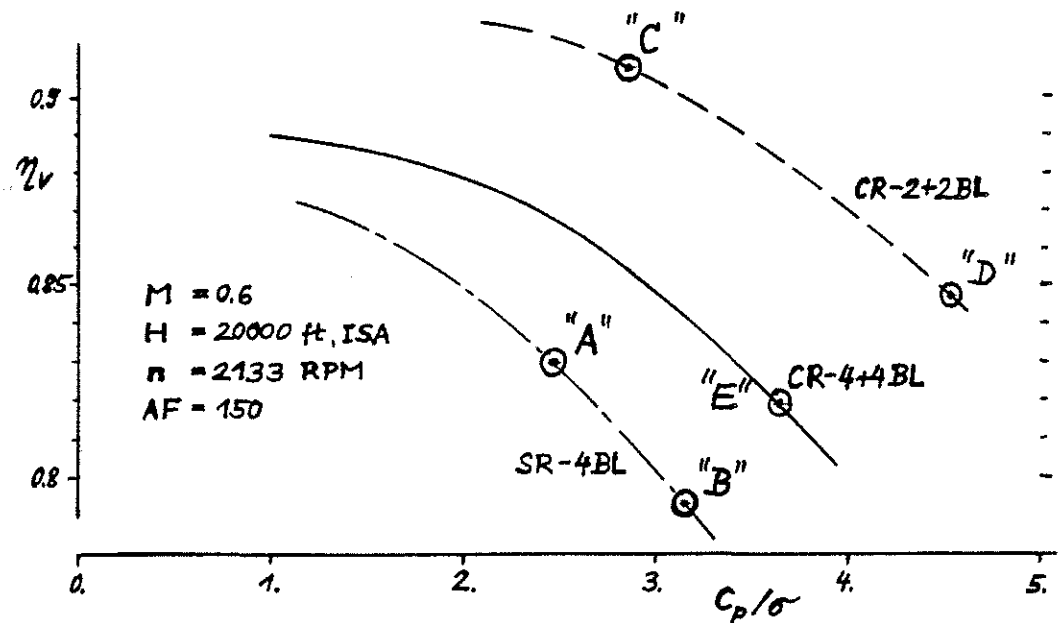
FIG. 29: Propulsive Efficiency of this Propeller in Cruise Condition
in Dependence of Blade Loading in Comparison with two
Coaxial Propellers with the same and twice the Solidity
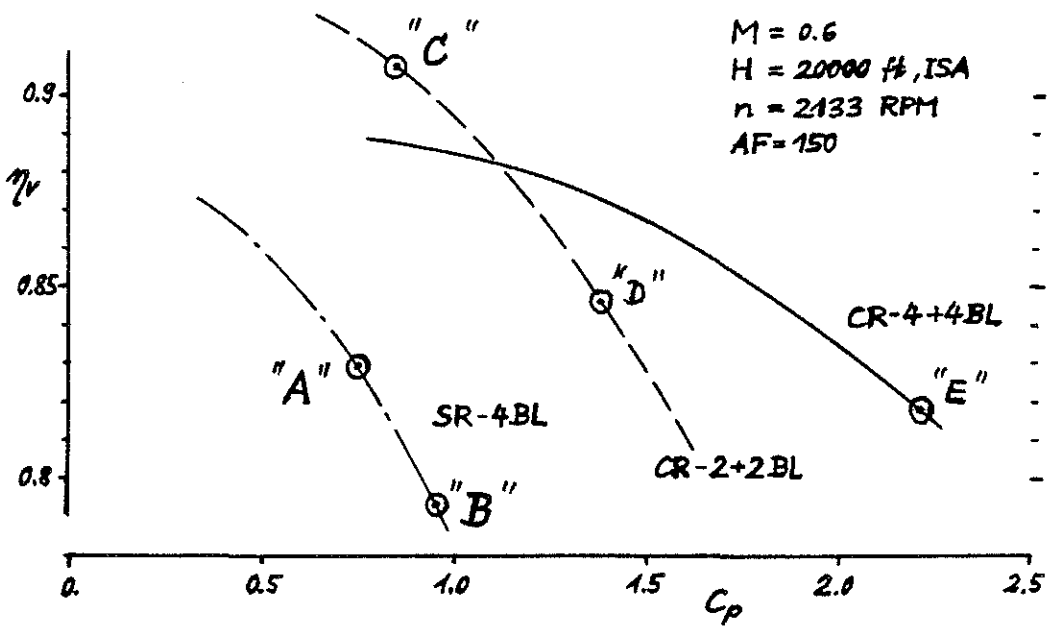
FIG. 30: Propulsive Efficiency of these Propellers in Cruise
Condition in Dependence of Power Loading
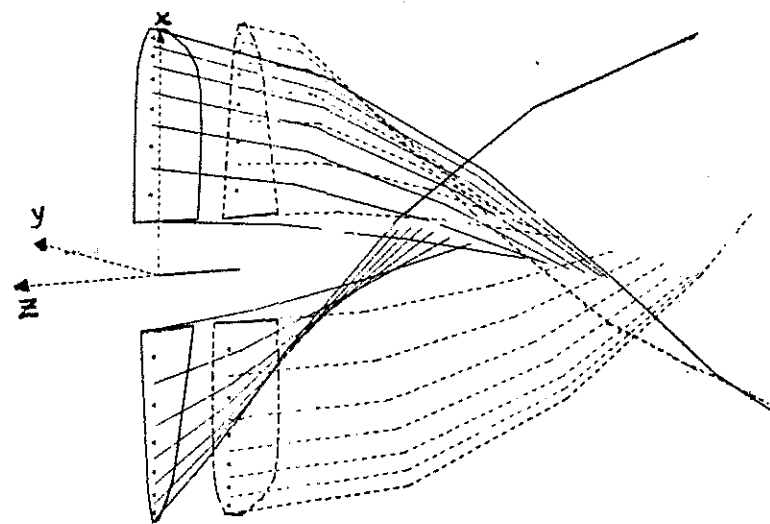
"D": $M = 0.6$

$H = 20000\,ft, ISA$

$n = 2133\,RPM$

$\vartheta_{75} = 53/55,5°$

$C_P = 1.3824$

$C_T = 0.4274$

$\eta_V = 0.8462$

$(12.0\ s.\ CPU)$
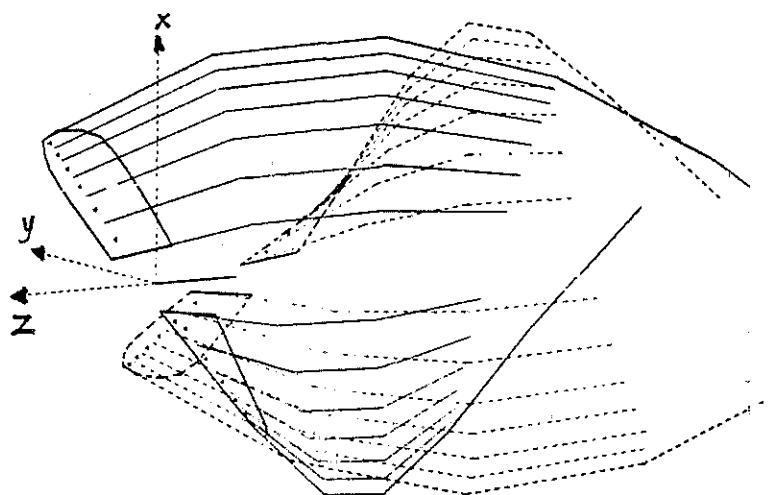
STEP 1:

$C_{P_1} = 1.4309$

$C_{T_1} = 0.4402$

STEP 2:

$C_{P_2} = 1.3678$

$C_{T_2} = 0.4237$
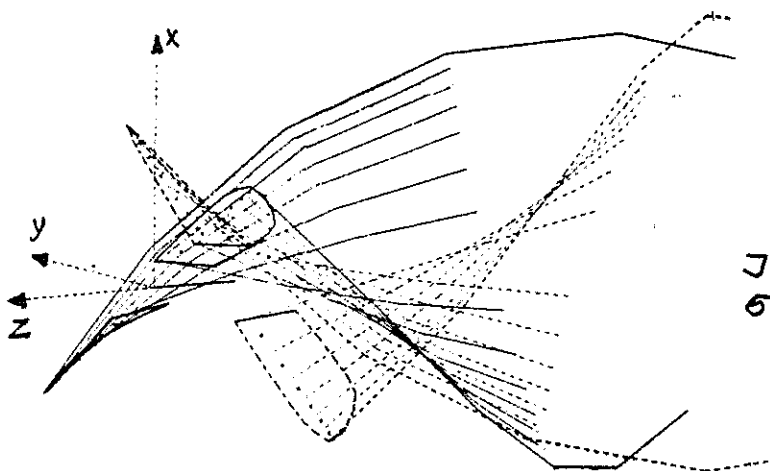
STEP 3:

$C_{P_3} = 1.3485$

$C_{T_3} = 0.4183$

$J = 2.74$

$\sigma = 0.301$

$P_2/P_1 = 0.97$

$T_2/T_1 = 0.86$

FIG. 31: Wake and Performance at Point "D" (Fig. 29, 30) in three
Time Steps of a Counter Rotating Propeller of the same
Solidity as the Propeller of Fig. 28 (CR-2+2 BL)
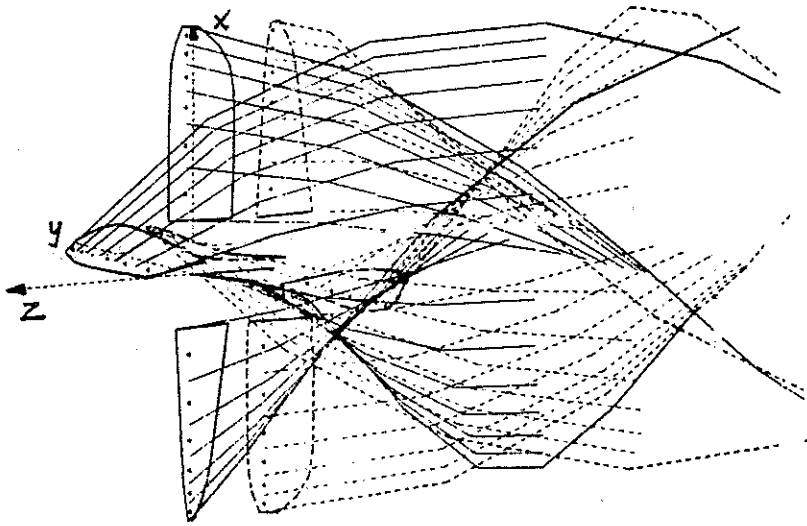
"E": $M = 0.6$

$H = 20000\ ft,\ ISA$

$n = 2133\ RPM$

$\vartheta_{75} = 52.5/56°$

$C_P = 2.2245$

$C_T = 0.6652$

$\eta_V = 0.8180$

$(36.0\ s.\ CPU)$
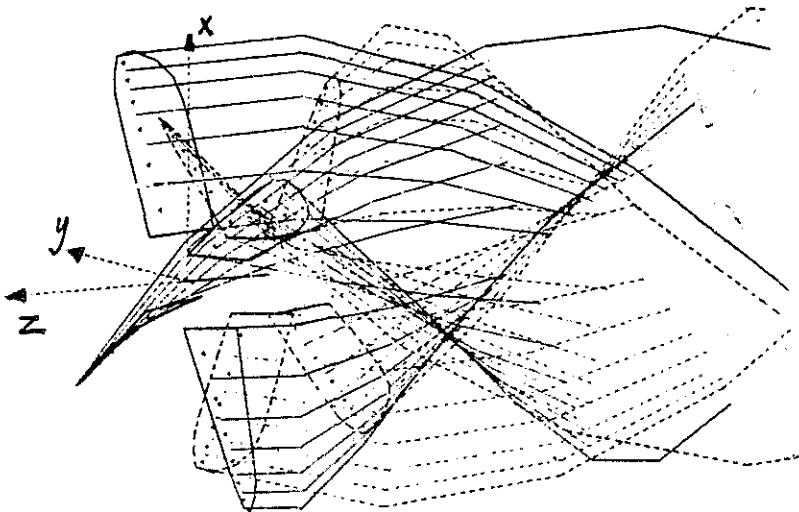
STEP 1:

$C_{P_1} = 2.2515$

$C_{T_1} = 0.6739$

STEP 2:

$C_{P_2} = 2.2218$

$C_{T_2} = 0.6650$
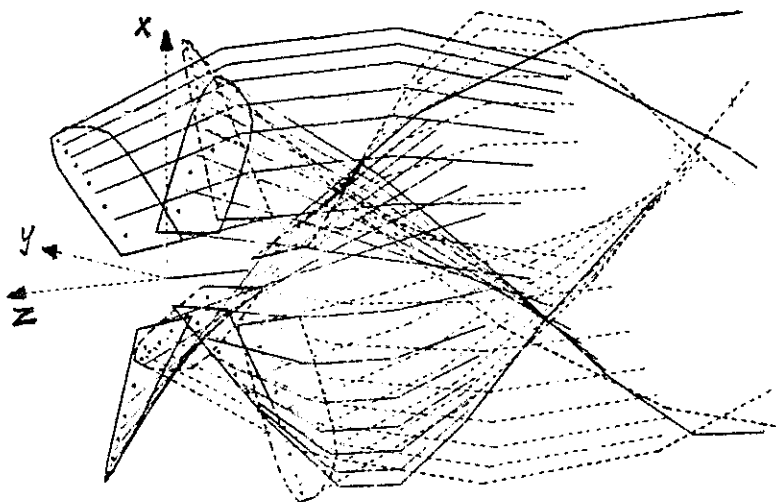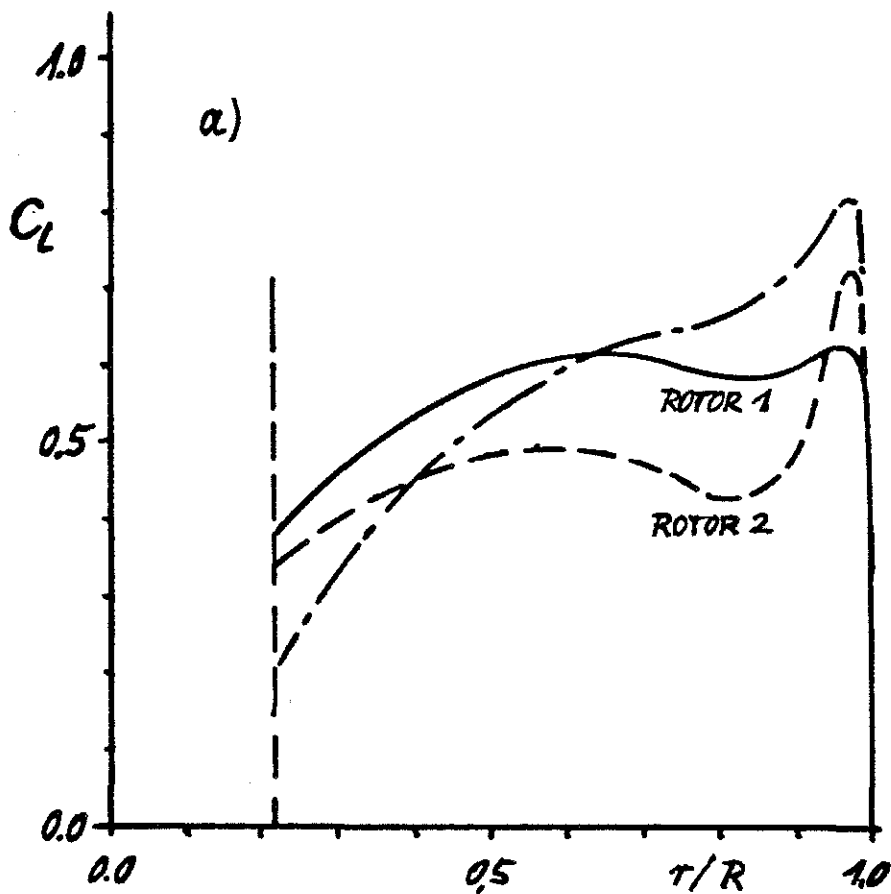
STEP 3:

$C_{P_3} = 2.2003$

$C_{T_3} = 0.6567$

$J = 2.74$
$\sigma = 0.602$

$P_2/P_1 = 0.993$

$T_2/T_1 = 0.86$

FIG. 32: Wake and Performance at Point "E" (Fig. 29, 30) in three Time Steps of a Counter Rotating Propeller of twice the Solidity as the Propeller of Fig. 28 (CR-4+4 BL)

a)

$M = 0.6$
$H = 20000 \, ft$, ISA
$n = 2133 \, RPM$

— · — "B"

SR - 4 BL, $\vartheta_{75} = 55°$

$C_T = 0.2774$

$C_P = 0.9579$

$\eta_v = 0.7926$

$\dfrac{ROTOR\ 1}{ROTOR\ 2}$ "C"

CR - 2+2 BL

$\vartheta_{75} = 50/52°$

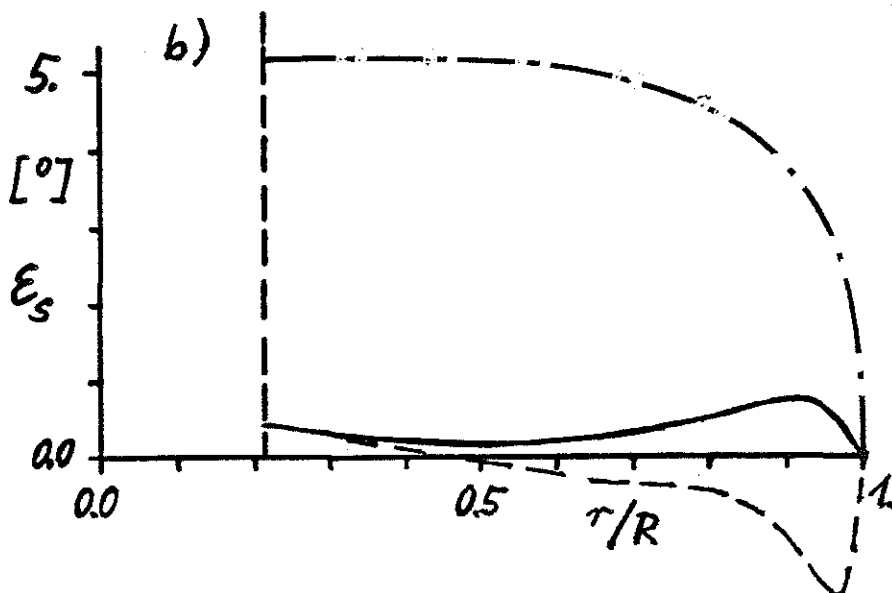$C_T = 0.2801$

$C_P = 0.844$

$\eta_v = 0.9083$

b)

FIG. 33: Comparison of the Local Lift Coefficient and Swirl Angle
of a Single Rotation and a Counter Rotation Propeller
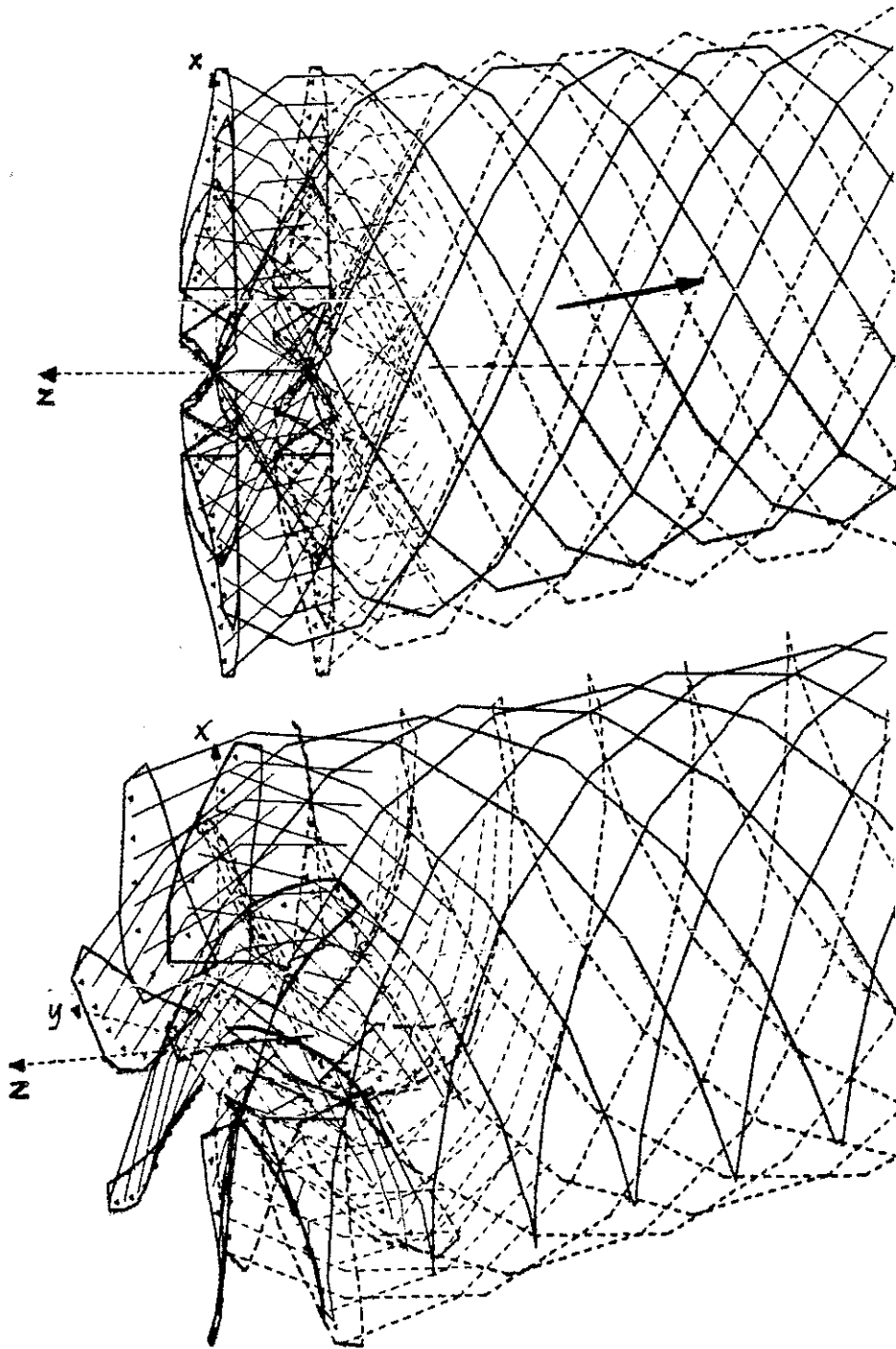at the same Solidity and Thrust (Points "B" and "C" in Fig. 29,30)

27-29

FIG. 34: Wake Model of a Counter Rotation Propfan at M = 0.3 in a 10 deg. skewed Flow Condition
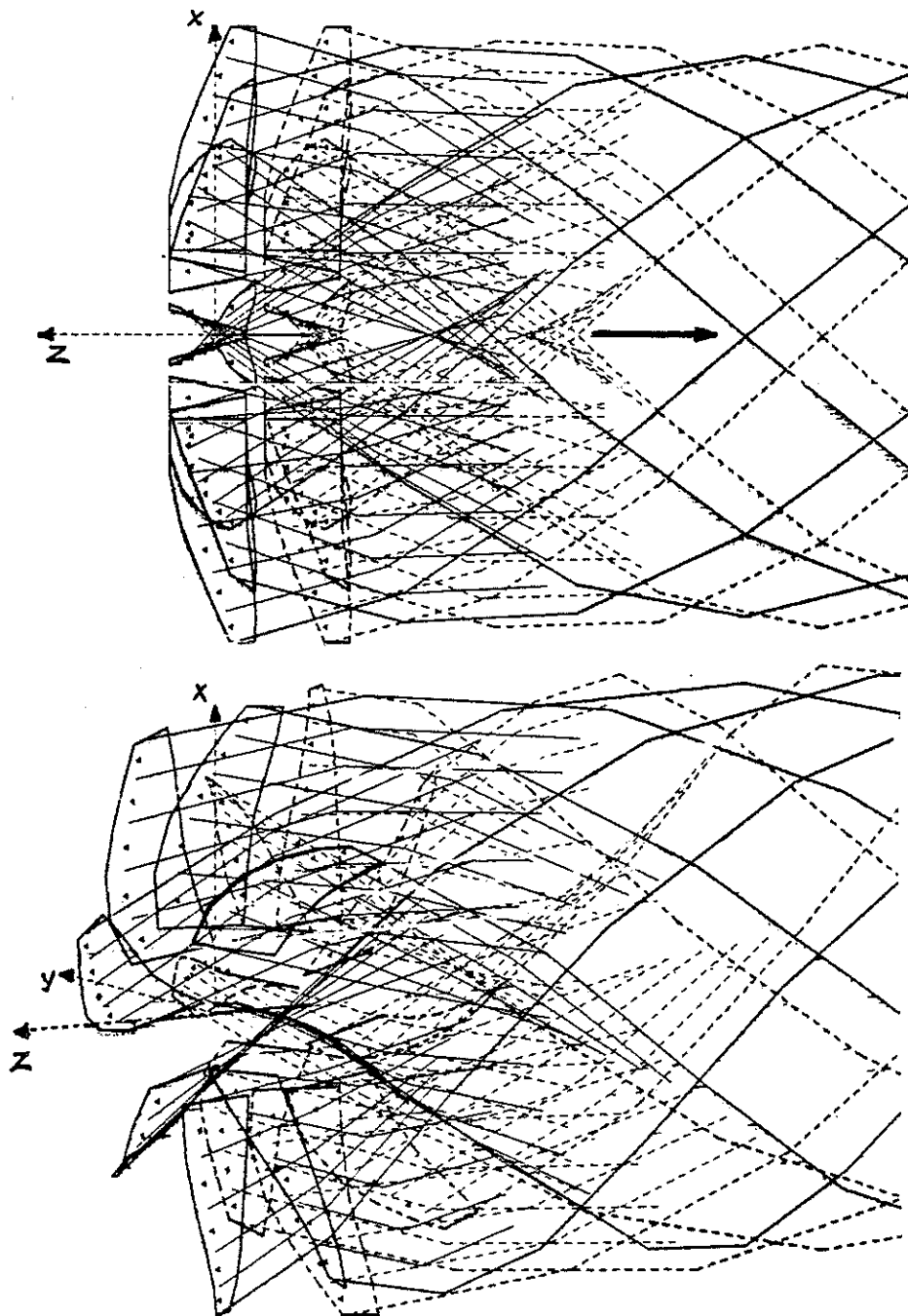
FIG. 35: Wake Model of a Counter Rotation Propfan at
M = 0.8 Cruise Condition